Quantum criticality around metal-insulator transitions of strongly correlated electron systems

Takahiro Misawa* and Masatoshi Imada
Department of Applied Physics, University of Tokyo, 7-3-1 Hongo, Bunkyo-ku, Tokyo, 113-8656, Japan
(Received 11 October 2006; revised manuscript received 26 December 2006; published 21 March 2007)

Quantum criticality of metal-insulator transitions in correlated electron systems is shown to belong to an unconventional universality class with violation of the Ginzburg-Landau-Wilson (GLW) scheme formulated for symmetry breaking transitions. This unconventionality arises from an emergent character of the quantum critical point, which appears at the marginal point between the Ising-type symmetry breaking at nonzero temperatures and the topological transition of the Fermi surface at zero temperature. We show that Hartree-Fock approximations of an extended Hubbard model on square lattices are capable of such metal-insulator transitions with unusual criticality under a preexisting symmetry breaking. The obtained universality is consistent with the scaling theory formulated for Mott transitions and with a number of numerical results beyond the mean-field level, implying that preexisting symmetry breaking is not necessarily required for the emergence of this unconventional universality. Examinations of fluctuation effects indicate that the obtained critical exponents remain essentially exact beyond the mean-field level. It further clarifies the whole structure of singularities by a unified treatment of the bandwidth-control and filling-control transitions. Detailed analyses of the criticality, containing diverging carrier density fluctuations around the marginal quantum critical point, are presented from microscopic calculations and reveal the nature as quantum critical "opalescence." The mechanism of emerging marginal quantum critical point is ascribed to a positive feedback and interplay between the preexisting gap formation present even in metals and kinetic energy gain (loss) of the metallic carrier. Analyses of crossovers between GLW type at nonzero temperature and topological type at zero temperature show that the critical exponents observed in $(V,Cr)_2O_3$ and κ-ET-type organic conductors provide us with evidence for the existence of the present marginal quantum criticality.

DOI: 10.1103/PhysRevB.75.115121 PACS number(s): 71.30.+h, 71.10.Fd

I. INTRODUCTION

Metal-insulator (MI) transitions in correlated electron systems have been a challenging subject of studies for decades.[1] In this paper, we show from microscopic analyses that MI transitions of correlated electrons bear an unconventional feature in view of quantum phase transitions. This is shown by taking an example of the Hartree-Fock approximation of the Hubbard model in two dimensions. One might suspect whether the Hartree-Fock approximations could yield a phase transition which is beyond the conventional scheme. However, we show that the simple mean-field approximation allows us to get insight into this issue by capturing the correct interplay of symmetry-breaking and topological characters of the transition. We also discuss that the unconventionality survives beyond the limitation of the mean-field study, where the scaling theory[2,3] formulated for the Mott transition is applicable. To make the motivation of the present study clearer, we describe a somewhat detailed introduction to clarify why the present study has significance and how the unconventionality arises in view of quantum phase transitions in general. Then, in the latter part of the Introduction, we review the previous studies of MI transitions to position the starting point.

A. General perspective in view of quantum phase transitions

A ubiquitous example of phase transitions seen in nature is the transition between gas and liquid. At the critical point of the gas-liquid phase transition, the compressibility

$$\kappa = -\frac{1}{V}\frac{dV}{dP} = \frac{1}{n}\frac{dn}{dP} = \frac{1}{n^2}\frac{dn}{d\mu} \tag{1}$$

and the equivalent density fluctuations $\int dr\langle n(r)n(0)\rangle$ diverge, where V and μ are the volume and chemical potential, respectively. The opalescence observed in light scattering is caused by such diverging density fluctuations. Nearly a century ago, the critical opalescence found in the scale of the light wavelength was analyzed by Ornstein and Zernike,[4] Einstein,[5] and Smoluchovski[6] as one piece of the evidence for the existence of atoms.

The gas-liquid transition is mapped to the ferromagnetic transition in the Ising model with the Z_2 symmetry expressed by the Hamiltonian

$$H = -J\sum_{\langle i,j\rangle} S_i S_j - h\sum_i S_i, \tag{2}$$

for the local spin S_i taking ± 1 at the site i and interacting with short-ranged neighbors at j and under the symmetry breaking field h. The Ising model represents the simplest example that phase transitions in general take place because of a spontaneous breaking of symmetries originally holding in the Hamiltonian at $h=0$. Although the gas-liquid transition at first glance does not look like it is breaking the symmetry as in the ordered phase of the Ising model, the transition is actually mapped to the Z_2 symmetry breaking along the first-order coexistence boundary. In fact, the up- and down-spin phases in the Ising model are mapped to the gas and liquid phases, respectively, from which both transitions turn out to belong to the same universality class. In more general terms,

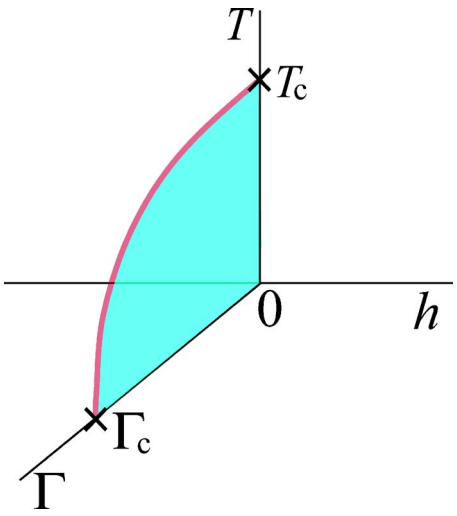

FIG. 1. (Color online) Schematic phase diagram of the Ising model under longitudinal and transverse magnetic fields h and Γ, respectively. Up- and down-spin phases are separated by the first-order boundary illustrated by shaded (blue) sheet below the critical line shown by the bold (brown) curve in parameter space of T and h and the transverse Ising field Γ. Beyond the quantum critical point at Γ_c, the transition disappears and the up- and down-spin phases are adiabatically connected even through the route on the $T=0$ plane.

thermal phase transitions are all characterized by a certain type of spontaneous symmetry breaking.

Phase transitions by conventional spontaneous symmetry breaking are correctly described by the Ginzburg-Landau-Wilson (GLW) scheme.[7–9] In this scheme, the free energy F is expressed by a functional of a spatially dependent order parameter $m(r)$ after eliminating other degrees of freedom. F is assumed to allow a regular expansion with respect to $m(r)$ such as

$$F = \int dr \left[-hm(r) + \frac{a}{2!}m(r)^2 + \frac{K}{2!}[\nabla m(r)]^2 + \frac{b}{4!}m(r)^4 + \cdots \right], \tag{3}$$

where b and K are positive constants and the coefficient a depends on the control parameter g around the critical point g_c as $a=a_0(g-g_c)$.

This classical picture of phase transitions is modified in quantum systems. For instance, when the transverse field $-\Gamma\Sigma_i S_i^x$ is additionally applied to the Ising model (2) by considering spin-1/2 quantum spins $\mathbf{S}_i=(S_i^x,S_i^y,S_i^z)$, T_c is suppressed to zero at a critical value Γ_c and the transition disappears as illustrated in Fig. 1. This may be regarded as a destruction of the symmetry-broken order by quantum fluctuations instead of thermal fluctuations.

In fact, a quantum system may be expressed in the path-integral formalism, where an additional dimension representing the imaginary-time or inverse-temperature axis is introduced in addition to the d-dimensional spatial degrees of freedom. Although the added imaginary-time direction could be qualitatively different from the spatial dimensions, one can show that it simply corresponds to z additional spatial dimensions, where z is called the dynamical exponent. The transverse Ising model is simply represented by $z=1$. Namely, the quantum phase transition at $T=0$ in d spatial dimensions realized by increasing Γ to Γ_c may be mapped to the transition at nonzero temperature in $(d+1)$-dimensional classical systems.[10]

However, in more general terms, if the quantum dynamics has a coupling to dissipative gapless excitations such as particle-hole excitations in metals, z may become larger than unity such as 2 or 3.[11–13] Ferromagnetic and antiferromagnetic phase transitions in metals have been extensively studied from this viewpoint. The quantum critical point appears when the critical temperature is lowered to zero. Around the quantum critical point, low-energy excitations arising from growing magnetic correlations have been proposed to cause non-Fermi-liquid properties.[11–13] A particular type of metamagnetic transitions has also been studied around the "quantum critical end point,"[14] where an apparent symmetry does not change at the critical point, whereas an implicit symmetry breaking does occur as in the case of the gas-liquid transition. Even in these cases with z larger than unity, however, the GLW scheme remains essentially valid when we consider a proper $(d+z)$-dimensional system.

Here the dynamical exponent z is defined from the ratio of the temporal correlation length ξ_t to the spatial one ξ of the order parameter $m(r,t)$ in d dimensions. In the case of conventional quantum phase transitions, ξ_t and ξ are defined by

$$\xi = -\lim_{r\to\infty}\left(\frac{\ln\langle m(r,0)m(0,0)\rangle}{r}\right)^{-1}, \tag{4}$$

$$\xi_t = -\lim_{t\to\infty}\left(\frac{\ln\langle m(0,t)m(0,0)\rangle}{t}\right)^{-1}, \tag{5}$$

respectively. More concretely, the dynamical exponent z is defined in the asymptotic limit to the critical point $g\to g_c$ by

$$z = \lim_{g\to g_c}\frac{\ln\xi_t}{\ln\xi}. \tag{6}$$

As we will show in the next subsection, in the case of the metal-insulator transitions, these definitions should be modified, because the correlations in metals decay not exponentially but with power laws as a function of distance in general.

In contrast to the description of the phase transition by symmetry breaking, several classes of quantum phase transitions at $T=0$ are not captured by such extensions of the GLW scheme and are not characterized by spontaneous symmetry breaking. One of the simplest examples is found in the transition between a metal and a band insulator. The ground-state energy E of noninteracting electrons near the parabolic band bottom with single-particle dispersion $\epsilon=Ak^2$ in d dimensions is obviously described by

$$E \propto n^{(d+2)/d} \propto \mu^{(d+2)/2} \tag{7}$$

in the metallic phase for the electron density n and the chemical potential μ measured from the band bottom. On the

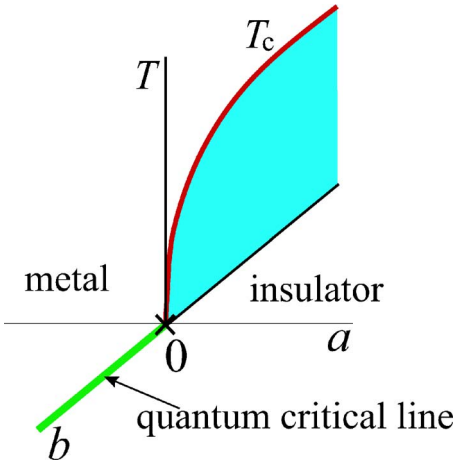

FIG. 2. (Color online) Proposed phase diagram of MI transitions for strongly correlated electron systems. A crucial difference from Fig. 1 is that the quantum critical line starts along the b axis [the thick (green) line along $a=T=0$] beyond the end point of the first-order boundary called the marginal quantum critical point depicted by the cross. This difference is a direct consequence of the topological nature of MI transitions at $T=0$. Here the first-order boundary is again shown by the shaded (blue) surface.

other hand, throughout the insulating phase with the chemical potential varied in the gap, $E=0$ holds because of $n=0$. This trivially nonanalytic form of the energy as a function of μ clearly represents a quantum phase transition with the singularity at $\mu=0$, but it is equally obvious that it does not follow the GLW scheme. This transition of noninteracting fermions is not accompanied by any kind of spontaneous symmetry breaking. It is rather characterized only by the presence or absence of the Fermi surface, which is a topological difference. Wen[15] has proposed a category of "quantum orders" for this class of transitions.

In this paper, we show that an involved interplay of a topological nature at $T=0$ with the conventional GLW character at $T\neq 0$ emerges for MI transitions of correlated electrons. By controlling a parameter for quantum fluctuations, a zero-temperature critical line characterized by the topological transition of the Fermi surface from a metal to an insulator switches over to a finite-temperature critical line characterized by the GLW scheme. The phase diagram is now seriously modified from Fig. 1 to a new type depicted in Fig. 2. Here, the quantum critical point is turned into the starting point (or end point) of the quantum critical line which represents the topological nature of transitions at $T=0$. We call this starting and marginal point shown as the cross in Fig. 2, the marginal quantum critical point (MQCP), which is completely different from the conventional quantum critical point. Then electron correlation effects generate an unconventional universality class of phase transitions, which is expected neither in GLW category nor in simple topological transitions.

B. Introduction for metal-insulator transitions

Now we summarize our current understanding of MI transitions for strongly correlated electrons achieved in previous studies in the literature to make clear our motivation of the present study. This issue has attracted long-standing interest and various important aspects have been clarified,[1] although complete understanding has not been reached. MI transitions may occur with coupling to lattice distortions or be accompanied by effects of randomness in real materials. However, the purely electronic origin of MI transitions has been a central issue in the strong-correlation regime, where we find many examples called Mott transitions. For this purpose, the Hubbard model, which only considers the local Coulomb interaction on a lattice, is one of the simplest models to describe MI transitions. The Hubbard model is defined by the Hamiltonian as

$$H = -\sum_{i,j,\sigma} t_{ij} c_{i\sigma}^{\dagger} c_{j\sigma} + U\sum_{i} n_{i\uparrow} n_{i\downarrow} - \mu\sum_{i} N_i, \tag{8}$$

where $c_{i\sigma}^{\dagger}$ ($c_{i\sigma}$) creates (annihilates) an electron with spin σ at site i, respectively. The number operator is $n_{i\sigma}$, and μ represents the chemical potential. The hopping integral between sites i and j is represented by t_{ij}, and U denotes the on-site Coulomb repulsion.

Approximate and simple theoretical descriptions of the Mott transition at $T=0$ without any symmetry breaking being involved were proposed in seminal works of Hubbard[16] and Brinkman and Rice.[17] These two works offer completely different pictures for the transition. The Hubbard approximation offers a picture of a simple splitting of a band into an upper and a lower band with a gap between these two bands. The transition to a Mott insulator occurs simply because the chemical potential moves into the gap. The "quasiparticle" weight Z at the Fermi level is retained as nonzero even at the transition, although the "large Fermi surface" with the Luttinger volume is not preserved and a small pocket of the Fermi surface shrinks to zero at the transition. The Brinkman-Rice picture obtained from the Gutzwiller approximation, in contrast, preserves the Luttinger volume, and the Mott insulator is realized by the vanishing quasiparticle weight Z. Dynamical mean-field theory[18] (DMFT) proposed some unification of these two pictures with the formation of the upper and lower Hubbard bands reproduced together with the vanishing Z in the coherent additional "band." In DMFT results, the Mott transition itself is triggered by the vanishing coherent band and the criticality is ultimately determined from that of the Brinkman-Rice scenario.

Recently, DMFT has been improved by taking into account the momentum dependence of the self-energy in the correlator projection method.[19] The Mott transition obtained from this improvement shows that a transition qualitatively different from the original DMFT scenario occurs, where the renormalization factor Z is kept nonzero until the transition.[20] Instead of vanishing Z, the transition is realized by shrinkage and vanishing of the Fermi-surface pocket with some similarity to the Hubbard picture. A crucial difference from the Hubbard picture is that the upper and lower Hubbard bands may have qualitatively different dispersions accompanied by electron differentiation in momentum space.[19,21,22] The vanishing pocket looks to show very anisotropic spectral weight with strong intensity on the inner-half circle and weak intensity on the outer-half circle, making an

apparent arc-type structure for the model on the square lattice. This arc-type structure is consistent with the experimental observations in the copper oxides obtained from angle-resolved photoemission spectroscopy (ARPES).[23,24] This Fermi-surface pocket appears after the Lifshitz transition within the metallic phase, where the topology of the Fermi surface changes from that of a large Fermi surface to pockets. Such Lifshitz transitions seem to inevitably occur, which invalidates the Luttinger theorem after the transition to the pockets.[20] A similar conclusion was obtained by cellular DMFT study for systems with a one-dimensional anisotropy,[25] as well as in two dimensions (2D),[26] and by a dynamical cluster approximation for 2D Hubbard model,[27] where the momentum dependence of the self-energy was considered in different ways. The serious modification of DMFT and the complete change in the nature of the MI transition with vanishing pockets of the Fermi surface seems to have a deep connection to satisfaction of the hyperscaling and a momentum-space differentiation as we discuss below.

A picture of MI transitions completely different from various mean-field approximations including DMFT has been proposed from the scaling theory of the Mott transition,[2,3] where the singularity of the free energy F at the Mott transition is assumed to follow the hyperscaling form

$$F \propto \xi^{-(d+z)}. \tag{9}$$

Here, ξ in the metallic side is the correlation length defined by $X^{-1/d}$ for the metallic carrier concentration X and spatial dimensionality d, while it is the localization length of carriers in the insulating side. A more precise definition of ξ should be given from the correlation length of the order-parameter correlation function, which will be discussed at the end of this section, and it will be clarified that the above relation is correct. The hyperscaling is normally satisfied below the upper critical dimension d_u, whereas the mean-field theories are satisfied above d_u. Therefore, the scaling theory and various mean-field theories are incompatible in general.

Before proceeding to more involved discussions of the scaling theory, we briefly summarize the basic points of critical phenomena and universality classes particularly for metal-insulator transitions used in the later discussions. The universality class of phase transitions is characterized by critical exponents. We first discuss relations for critical exponents which are applicable irrespective of the validity of either the hyperscaling or mean-field approximations. When we take the carrier concentration X as the order parameter in the metallic side, the critical exponent δ is defined by

$$X \propto \zeta^{1/\delta}, \tag{10}$$

which measures the scaling behavior of the growth of the order parameter as a function of the field ζ, which is conjugate to the order parameter X. Namely, ζ is either the chemical potential μ for the filling-control transition or U/t in the Hubbard model for the bandwidth control transition. In the latter case, ζ is, for example, controlled by the pressure P in actual experiments. The carrier concentration X is the doping concentration itself for the filling-control case while it is the unbound doublon (doubly occupied sites) and holon (empty site) concentrations measured from values at the critical point for the bandwidth-control case.

The exponent ν is defined from the relation of the control parameter g to ξ as

$$\xi \propto |g - g_c|^{-\nu}. \tag{11}$$

Here, the control parameter g may also be controlled by U/t or μ, which makes some complexity and could cause confusion, because these two quantities can control both ζ and g. This is somehow in contrast with the simple case of Eq. (3), where h and a may be controlled independently—say, by the magnetic field and temperature, respectively. In the later microscopic description in Sec. III, this somewhat confusing situation will be resolved.

The exponent γ is defined from the order-parameter susceptibility $\chi = dX/d\zeta$ from the scaling

$$\chi \propto |g - g_c|^{-\gamma}. \tag{12}$$

The jump of X at the first-order boundary grows from the critical point as

$$X \propto |g - g_c|^{\beta}. \tag{13}$$

The exponent α is obtained from the second derivative of the free energy as

$$d^2F/dg^2 \propto |g - g_c|^{-\alpha}. \tag{14}$$

It should be noted that α for quantum phase transitions does not express the exponent for the specific heat as in thermal transitions. The set of these exponents has a significant meaning because the set specifies the fundamental nature of the phase transitions called the universality class.

Conventional scaling laws such as Widom's law

$$\beta(\delta - 1) = \gamma \tag{15}$$

and Rushbrooke's law

$$\alpha + 2\beta + \gamma = 2 \tag{16}$$

may be satisfied for these exponents. So far, the control parameter g is not fixed yet and one may have several choices. Some of the exponents need trivial transformations depending on the definition of g.[28]

When the hyperscaling assumption is employed, the length scale which diverges toward the critical point is unique, and it must be the mean carrier distance given by

$$\xi \propto X^{1/d}. \tag{17}$$

Then the free energy expressed by Eq. (9) leads to

$$F \propto X^{(d+z)/d}. \tag{18}$$

This is the form at $\zeta = 0$ and $g - g_c = 0$. Scaling relations are derived by further adding the term of the "chemical potential" ζ and the term of coupling to $g - g_c$ as

$$F = -\zeta X + B_0(g - g_c)X^{\phi} + CX^{(d+z)/d}, \tag{19}$$

where B_0 and C are constants and ϕ should be separately given from a physical consideration or microscopic derivation of the transition. Note that the definition of g is now fixed as the quantity to control the transition at $\zeta = 0$. The

scaling between X and ζ—namely, Eq. (10)—is obtained by putting $g-g_c=0$ in Eq. (19) and minimizing the free energy by $dF/dX=0$. This yields

$$\delta = z/d. \tag{20}$$

The scalings between X and g—namely, Eqs. (12) and (13)—are obtained by putting $\zeta=0$ in Eq. (19) and minimizing the free energy by $dF/dX=0$. This yields

$$\beta = \frac{1}{1-\phi+z/d} \tag{21}$$

and

$$\gamma = \frac{z-d}{z+d(1-\phi)}. \tag{22}$$

From Eqs. (11), (13), and (17), a further relation

$$\nu = \beta/d \tag{23}$$

is obtained. Note that the scaling laws, Eqs. (15) and (16), are obviously satisfied for Eqs. (20)–(23). From the scalings (9), (11), and (17), we obtain $F \propto |g-g_c|^{\nu(d+z)}$ for nonzero $g-g_c$. From this and Eq. (14), the Josephson relation

$$\alpha = 2-\nu(d+z) \tag{24}$$

is obtained. In addition, the Drude weight is shown to follow[1]

$$D \propto X^{1+(z-2)/d}. \tag{25}$$

To estimate accurate exponents of microscopic models, in principle, one needs to go beyond the mean-field approximation, because the reliability of the mean-field approximation itself has to be critically tested. Available theoretical tools for this purpose are severely limited because of various difficulties in theoretical approaches for strongly correlated electrons. In the literature, there exist only a small number of available estimates from unbiased approaches such as the quantum Monte Carlo and path-integral renormalization group methods. For the filling-control transition of the Hubbard model or the t-J model on a square lattice, by using the quantum Monte Carlo method[29–31] and power Lanczos method,[32] the charge compressibility has been shown to follow the scaling $dX/d\mu \propto X^{-1}$, from which δ is estimated from Eq. (10) as $\delta \sim 2$. The result obtained from the path-integral renormalization group method is also consistent with this scaling.[33] When the hyperscaling holds, $\delta=2$ and Eq. (20) in two dimensions leads to $z=4$. On the other hand, the simple GLW scheme always gives $\delta>3$ and is incompatible with the numerical results. In fact, the exponents of the Ising model are $\delta \sim 4.8$ for three-dimensional systems and $\delta=15$ in two dimensions. Any other types of symmetry breakings indicate $\delta>3$. Note also that the degeneracy temperature (effective Fermi temperature) T_F is scaled by $T_F \propto \xi^{-z} \propto X^{z/d}$, resulting in $T_F \propto X^2$ for $z=4$ and $d=2$, if the hyperscaling is satisfied.[3]

Experimentally, the exponent δ has been examined for filling-control transitions by measuring the chemical potential shift with increasing doping by photoemission studies in several high-T_c copper oxides.[34,35] In particular, $Bi_2Sr_2CaCu_2O_{8+y}$ and $(La,Sr)_2CuO_4$ show pinnings of the chemical potential at low doping, indicating an enhancement of the charge compressibility and consistency with $\delta=2$. ^{3}He adsorbed on a graphite surface, offering a unique two-dimensional fermion system with strong correlation effects, appears to show an anomalous suppression of T_F near the commensurate solid phase in accordance with the trend of $T_F \propto X^2$, consistently with $z=4$,[36] with the hyperscaling being satisfied.

In addition, the Drude weight has been calculated to be consistent with $D \propto X^2$,[37,38] which suggests $z=4$ from the above relation (25) if the hyperscaling is satisfied. These two independent estimates of z coincide with each other and support the hyperscaling.

Other exponents are directly related to the g dependence of F, and it is fixed when ϕ is specified. If one put $z=4$ and $d=2$,

$$\nu = \frac{1}{2(3-\phi)}, \tag{26}$$

$$\alpha = 2-3\frac{1}{3-\phi}, \tag{27}$$

$$\beta = \frac{1}{3-\phi}, \tag{28}$$

and

$$\gamma = \frac{1}{3-\phi} \tag{29}$$

are obtained.

This unconventional universality class has further been analyzed, and $\phi=2$ is obtained from a plausible assumption on the quasiparticle dispersion.[39–41] Then, the universality class is proposed to be characterized by a set of the exponents

$$z=4, \quad \alpha=-1, \quad \beta=1, \quad \gamma=1, \quad \delta=2, \quad \nu=1/2, \quad \eta=0. \tag{30}$$

At finite temperatures, it has been theoretically proposed that the MI transition is equivalent to the gas-liquid transition and its universality class belongs to the Ising universality class.[42,43] Experimentally, from a recent careful study of V_2O_3 by Limelette *et al.*,[44] they have obtained the critical exponents which are consistent with that of the 3D Ising model—namely, $\beta \sim 0.34$, $\delta \sim 5.0$, and $\gamma \sim 1.0$—in the region very close to the critical point, whereas, except for its close vicinity, they have obtained consistency with the mean-field exponents for the Ising model in a wide region around the critical point. On the contrary, recent experimental results on κ-$(ET)_2Cu[N(CN)_2]Cl$ (Refs. 45 and 46) indicate the critical exponents $\beta=1$, $\gamma=1$, and $\delta=2$, which are consistent with Eq. (30) and indicate evidence for the relevance of the present universality.

Before closing this section, we remark on the definition of ξ and the dynamical exponent z. In the case of MI transitions, correlation functions do not decay exponentially as a

function of distance in the metallic phase. Therefore, the conventional definition of ξ given in Eq. (4) is not applied. For example, noninteracting electrons have a density-density correlation function $\langle X(r)X(0)\rangle$ which asymptotically decays as $1/r^3$ with Friedel oscillations in two dimensions.[30] Such an asymptotic decay crosses over to a constant at a shorter distance, where the crossover length is determined from the inverse of the Fermi wave number k_F. Since $1/r^3$ decay is absolutely convergent in the integration, the integration over distance is contributed dominantly from the region inside of the length scale of k_F^{-1}. From this, ξ is given by $\xi \propto k_F^{-1} \propto X^{-1/d}$. More precisely, the correlation length ξ is defined by

$$\xi \equiv \sqrt[d]{\frac{\int dr\langle X(r,0)X(0,0)\rangle}{\langle X(0,0)X(0,0)\rangle}}. \tag{31}$$

In a similar way, the temporal correlation length ξ_t is defined by

$$\xi_t = \frac{\int dt\langle X(0,t)X(0,0)\rangle}{\langle X(0,0)X(0,0)\rangle}. \tag{32}$$

Then the dynamical exponent z is obtained from

$$z = \lim_{g\to g_c} \frac{\ln \frac{\chi}{S}}{\ln \xi}, \tag{33}$$

where we have used relations for the equal-time structure factor S and susceptibility χ, given by

$$S \equiv \int dr\langle X(r,0)X(0,0)\rangle \propto \xi^{-d}, \tag{34}$$

$$\chi \equiv \int dr\, dt\langle X(r,t)X(0,0)\rangle \propto \xi^{z-d}, \tag{35}$$

leading to

$$\frac{\chi}{S} \propto \xi^z. \tag{36}$$

C. Outline of the present work

In this paper, we show that the basic structure of the phase diagram for the MI transition involving the quantum critical line and the boundary for the first-order transition is correctly captured by the Hartree-Fock theory of the Hubbard model. A remarkable result in this paper is that the Hartree-Fock approximation is able to derive the above unconventional universality class at the MQCP from a microscopic derivation of the free energy. The obtained universality class turns out to be consistent with the scaling theory. The mechanism of the emergence of the MQCP and resultant unconventional universality is clarified in the present microscopic study. It is ascribed to the self-consistent positive feedback between the metallic carrier density and the amplitude of an insulating gap already developed in metals. More concretely, an increase of the preformed gap amplitude decreases the carrier density to lower the kinetic energy, which in turn further enhances the preformed gap. On the contrary, the decreasing preformed gap allows more carriers, which further reduce the gap to gain the kinetic energy of carriers. These nonlinear effects cause the first-order transition and the MQCP emerges at the border between the first-order transition and the quantum critical line. Furthermore, the Hartree-Fock theory turns out to remain essentially correct even when one goes beyond the mean-field approximation and takes into account quantum fluctuations. This is because the transition always occurs as that at the upper critical dimension irrespective of the spatial dimensionality. We further show that the Hartree-Fock solution has a finite-temperature crossover to the conventional Ising universality class. We discuss implications and consequences of this unexplored type of universality class emerging near the MQCP sandwiched by GLW critical and quantum critical lines. We argue that low-energy excitations are described neither by the original single-particle picture nor by the bosonic density fluctuations when both characters of transitions meet.

We also discuss a comparison of the present result with the experimental indications obtained so far. It is shown that the critical exponents at the MQCP together with the finite-temperature crossover are completely consistent with whole aspects of the experimental results.

A part of the discussions in this paper has already been briefly given.[47] In this paper, we present the results of quantum MI transitions in greater detail. In particular, we show details of the procedure to obtain the non-GLW free-energy expansion and critical exponents together with thorough discussions on implications.

The organization of this paper is as follows: In Sec. II, we show details of our Hartree-Fock approximation. In Sec. III, we present Hartree-Fock solutions of the MI transition by introducing the preexisting order parameter. It captures some essence of the unconventional universality class of the transition from metals to insulators caused by electron correlation effects. Using the free-energy expansion, we analytically obtain the critical exponents of quantum MI transitions, which belong to an unconventional universality. We also discuss implications beyond the mean-field approximations in Sec. III. In Sec. IV, we show numerical results of the Hartree-Fock approximation at $T=0$, which are completely consistent with the analytical results in Sec. III. In Sec. V, the finite-temperature crossover is calculated. It shows a well-defined crossover from the Ising universality in the close vicinity of the critical point to the quantum universality governed by the MQCP when the parameter deviates from the critical point. Section VI describes comparisons of the present implications with relevant experimental results. Section VII is devoted to a summary and discussion.

II. HARTREE-FOCK APPROXIMATION

In this paper, to capture the essence of quantum MI transitions, we extend the Hubbard model (8) by considering the nearest-neighbor repulsion term proportional to V on the $N_s=L\times L$ square lattice. It is defined by

$$H = \sum_{k,\sigma} [\xi_1(\mathbf{k}) + \xi_2(\mathbf{k})] c^\dagger_{k\sigma} c_{k\sigma} + U \sum_i n_{i\uparrow} n_{i\downarrow} + V \sum_{\langle ij \rangle} N_i N_j - \mu \sum_i N_i, \tag{37}$$

where $N_i = (n_{i\uparrow} + n_{i\downarrow})$ are number operators. We restrict the hopping terms to the nearest-neighbor pairs given by the dispersion $\xi_1(\mathbf{k}) = -2t(\cos k_x + \cos k_y)$ and that of the next-nearest-neighbor pairs by $\xi_2(\mathbf{k}) = 4t' \cos k_x \cos k_y$, respectively.

Using this extended Hubbard model, we study quantum MI transitions in a two-dimensional system within the Hartree-Fock approximation. Although Hartree-Fock analyses have been done for the Hubbard model in the literature,[48,49] the criticality of MI transitions has not been examined. By considering the MI transitions in the ordered phase, we are able to capture a remarkable aspect of MI transitions from a microscopic model.

To consider the MI transitions within the Hartree-Fock approximation, we consider a symmetry-broken long-range order such as charge or antiferromagnetic (AF) ordering with the periodicity commensurate to the lattice. Then we study the MI transitions in the symmetry-broken phase. We note that the essence of the MI transitions does not depend on the type of ordering. For the extended Hubbard model defined in Eq. (37), two simple orders become stable. When $4V > U$, the extended Hubbard model has a tendency to charge ordering, where the empty and doubly occupied sites alternatingly align within the mean-field level. The order parameter m of checker-board-type doublon alignment is defined by

$$m = \frac{1}{N_s} \sum_i \langle (n_{i\uparrow} + n_{i\downarrow}) \exp(i\mathbf{Q} \cdot \mathbf{r}_i) \rangle, \tag{38}$$

where $\mathbf{Q}$ is the ordering wave vector (π, π). For $U > 4V$, the antiferromagnetic ordering becomes stable. The order parameter of the antiferromagnetic ordering m_{AF} is defined by

$$m_{\mathrm{AF}} = \frac{1}{N_s} \sum_i \langle (n_{i\uparrow} - n_{i\downarrow}) \exp(i\mathbf{Q} \cdot \mathbf{r}_i) \rangle. \tag{39}$$

Hereafter, we mainly consider the charge ordering. However, within the mean-field approximation, the antiferromagnetic order and charge order play the same role in the MI transition, and by replacing the order parameter m with the antiferromagnetic one, one can easily reach the same results for the nature of the MI transition.

Here we take the mean field as

$$\langle n_{i\uparrow} \rangle = \langle n_{i\downarrow} \rangle = \frac{n + m \exp(i\mathbf{Q} \cdot \mathbf{r}_i)}{2}, \tag{40}$$

with n being the average charge density given by $1/N_s \Sigma_i \langle n_{i\uparrow} + n_{i\downarrow} \rangle$. Using this mean field, we decouple the interaction term.

The on-site interaction term is decoupled as

$$U \sum_i n_{i\uparrow} n_{i\downarrow} \sim U \sum_i (n_{i\uparrow} \langle n_{i\downarrow} \rangle + n_{i\downarrow} \langle n_{i\uparrow} \rangle - \langle n_{i\uparrow} \rangle \langle n_{i\downarrow} \rangle) = \frac{U}{2} \sum_{i\sigma} [n_{i\sigma} (n + m e^{i\mathbf{Q} \cdot \mathbf{r}_i})] - \frac{U N_s (n^2 + m^2)}{4}. \tag{41}$$

The nearest-neighbor interaction term is decoupled as

$$V \sum_{\langle ij \rangle} N_i N_j \sim V \sum_{\langle ij \rangle} (N_i \langle N_j \rangle + N_j \langle N_i \rangle - \langle N_i \rangle \langle N_j \rangle) = 4nV \sum_i N_i - 4mV \sum_i N_i \exp(i\mathbf{Q} \cdot \mathbf{r}_i) - 2VN_s(n^2 - m^2). \tag{42}$$

Finally we obtain a Hartree-Fock Hamiltonian (H_{HF}) in the momentum space as

$$H_{HF} = \sum_{k,\sigma} \left(\epsilon(\mathbf{k}) + \frac{Un}{2} + 4nV - \mu \right) c^\dagger_{\mathbf{k}\sigma} c_{\mathbf{k}\sigma} + \left(\frac{U}{2} - 4V \right) m \sum_{\mathbf{k}\sigma} c^\dagger_{\mathbf{k}+Q\sigma} c_{\mathbf{k}\sigma} - \left(\frac{UN_s(n^2 + m^2)}{4} + 2VN_s(n^2 - m^2) \right), \tag{43}$$

where we define $\epsilon(\mathbf{k}) = \xi_1(\mathbf{k}) + \xi_2(\mathbf{k})$.

Diagonalizing the Hamiltonian leads to two bands of the form

$$E_\pm = \xi_2(\mathbf{k}) \pm \sqrt{\xi_1(\mathbf{k})^2 + \Delta^2} - \mu, \tag{44}$$

where $\Delta = mg$, and we now take $g = 4V - \frac{U}{2}$ as the control parameter, because in this section we mainly consider the bandwidth-control transition. In Eq. (44), we dropped a constant term $n(g+U)$.

Using this Hartree-Fock band dispersion we obtain the free energy

$$F_{HF} = -\frac{T}{N_s} \ln Z_{HF} = -\frac{2T}{N_s} \sum_{\mathbf{k},\eta} \ln \left[1 + \exp\left(-\frac{E_\eta(\mathbf{k})}{T} \right) \right] - \left(\frac{U(n^2 + m^2)}{4} + 2V(n^2 - m^2) \right), \tag{45}$$

where the suffix η takes $\pm$.

From this free energy, the order parameter m is determined from the self-consistency condition

$$\frac{1}{g} = \frac{2}{N_s} \sum_{\mathbf{k}} \frac{f(E_-(\mathbf{k})) - f(E_+(\mathbf{k}))}{E_+(\mathbf{k}) - E_-(\mathbf{k})}, \tag{46}$$

where $f(x)$ is the Fermi-Dirac distribution function. The particle density n is given by

$$n = \frac{1}{N_s} \sum_{\mathbf{k}} f(E_-(\mathbf{k})) + f(E_+(\mathbf{k})). \tag{47}$$

Details of the numerical calculations of Eqs. (46) and (47) are given in Appendix A.

It turns out that the self-consistent equation (46) with Eq. (44) for the charge ordering is equivalent to the self-consistent equation for the AF ordering defined in Eq. (39).[48,49] The equivalence holds by replacing the charge order parameter m with the AF order m_{AF} and by putting $g=U/2$. However, one should be careful about this mapping. This mapping is complete only on the Hartree-Fock level. The charge ordering at the (π,π) periodicity is the consequence of the discrete symmetry breaking while the AF ordering is realized by the continuous symmetry breaking of SU(2) symmetry. Therefore, if it would be exactly solved in two-dimensional systems, the charge ordering can indeed exist at finite temperatures, though AF ordering cannot exist at finite temperatures by the Mermin-Wargner theorem. Therefore, the Hartree-Fock approximation captures some essence of the charge ordering at finite temperatures, while the AF ordering at nonzero temperatures in two dimensions contains an artifact of the Hartree-Fock approximation, although the development of the charge gap itself is not an artifact, which leads to the Mott gap formation even without any long-range order. The physics of unconventional quantum criticality, which we clarify later, emerges from the gap formation itself and therefore the essence is captured in the Hartree-Fock calculation.

III. FREE-ENERGY EXPANSION AND CRITICAL EXPONENTS

In this section, we analyze singularities of the free energy around the MI transition within the Hartree-Fock approximation at $T=0$ and obtain the critical exponents of the transition. When the order parameter m and the gap $\Delta=mg$ are sufficiently small near the charge-order or antiferromagnetic transition, the insulating gap does not open for nonzero positive t'. This is because the upper band E_+ and lower band E_- overlap for a small gap. From Eq. (44), the top [bottom] of the lower [upper] band is located at $(k_x,k_y)=(\pi/2,\pi/2)$ $[(\pi,0)]$, respectively. The continuous MI transition occurs when the top of the lower band reaches the same energy as that of the bottom of the upper band as shown in Fig. 3. Therefore, the condition of the continuous MI transition is given by

$$E_+(\pi,0,\Delta_c)=E_-(\pi/2,\pi/2,\Delta_c), \tag{48}$$

where Δ_c is the critical gap of the continuous MI transition. From this, at $T=0$, we obtain the critical gap Δ_c as

$$\Delta_c=2t'. \tag{49}$$

This quantum MI transition occurs between charge-ordered metal and charge-ordered insulator; thus, the symmetry does not change at the transition. It is legitimate to expand the free energy around the nonzero order parameter measured from the critical point of the MI transition. One might speculate that the free energy expressed only by the order parameter Δ in Eq. (45) would be regular around the MI transition. However, as we will see below, this expansion has a piecewise analytic form in the metallic and insulating phases separately with a jump of the expansion coefficient at the transition point. This somewhat unconventional form of expansion is derived from the fact that some of the expansion coefficients explicitly depend on the density of states at the Fermi level, which has a discontinuity at the MI transition. This free-energy structure with a jump is in a complete contrast with the GLW form.

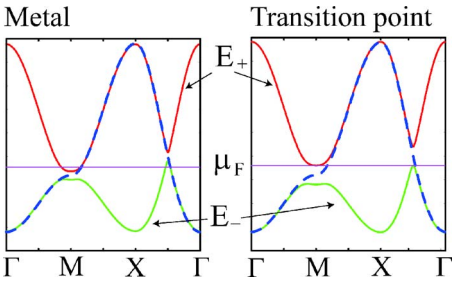

FIG. 3. (Color online) Quasiparticle band structures of the Hartree-Fock solution for the metallic phase (left) and the continuous MI transition point (right) are shown. The dashed (blue) line shows the free-particle band dispersion defined by $\epsilon(\mathbf{k})=-2t(\cos k_x+\cos k_y)+4t'\cos k_x\cos k_y$. The definition of the upper (lower) band is defined in Eq. (44). Fermi energy μ_F is represented by the horizontal line. In the metallic phase, the bottom of the upper band at the M point $[(\pi,0)$ and its equivalent points] is lower than the top of the lower band at $(\pi/2,\pi/2)$ and its equivalent points so that the indirect insulating gap is closed.

In this section, we consider the bandwidth-control transition at half filling $(n=1)$ in the canonical ensemble. In the scheme of the canonical ensemble, we add a term μn to the free energy defined in Eq. (45). The Hartree-Fock free energy F_{CHF} is given by

$$F_{CHF}=-\frac{2T}{N_s}\sum_{\mathbf{k},\eta}\ln\left[1+\exp\left(-\frac{E_\eta(\mathbf{k})}{T}\right)\right]+\frac{\Delta^2}{2g}+\mu n, \tag{50}$$

where η runs over $+$ and $-$. Hereafter, we describe F_{CHF} as F.

A. Free-energy expansion

Since the Δ dependence of F is explicitly given in Eq. (50), it allows a formal expansion of F in terms of Δ around a nonzero value Δ_c by taking an expansion parameter $Y=\Delta_c-\Delta$. The region $Y>0$ $(Y<0)$ represents the metallic phase (insulating phase), respectively. The form of expansion is given as

$$F(\Delta)=F(\Delta_c)+AY+\frac{B}{2!}Y^2+\frac{C}{3!}\Delta Y^3+\cdots, \tag{51}$$

where the coefficients are given by

$$A=-\left.\frac{\partial F}{\partial\Delta}\right|_{\Delta=\Delta_c}=-\left(\frac{1}{g}-W_1\right)\Delta_c, \tag{52}$$

$$B = \left.\frac{\partial^2 F}{\partial \Delta^2}\right|_{\Delta=\Delta_c} = \frac{1}{N_s}\sum_{\mathbf{k},\eta}\left.\left(\frac{\partial f(E_\eta(\mathbf{k},\Delta))}{\partial\Delta}\frac{\Delta}{\eta\sqrt{\xi_1^2+\Delta^2}}\right)\right|_{\Delta_c} - W_2, \quad (53)$$

$$C = -\left.\frac{\partial^3 F}{\partial \Delta^3}\right|_{\Delta=\Delta_c} = -\frac{1}{N_s}\sum_{\mathbf{k},\eta}\left.\left(\frac{\partial^2 f(E_\eta(\mathbf{k},\Delta))}{\partial\Delta^2}\frac{\Delta}{\eta\sqrt{\xi_1^2+\Delta^2}}\right)\right|_{\Delta_c} - 3W_3, \quad (54)$$

with the definitions

$$W_1 = v_1, \quad (55)$$

$$W_2 = v_1 - \Delta_c^2 v_3, \quad (56)$$

$$W_3 = v_3\Delta_c - v_5\Delta_c^3. \quad (57)$$

Here, v_n is defined by

$$v_n = -\frac{1}{N_s}\sum_{\mathbf{k},\eta}\eta(\xi_1^2+\Delta_c^2)^{-n/2} f(E_\eta(\mathbf{k},\Delta_c)). \quad (58)$$

To derive Eqs. (53) and (54), we neglect terms proportional to

$$\frac{\partial f(E_\eta(\mathbf{k},\Delta))}{\partial\Delta}\frac{\partial}{\partial\Delta}\left.\left(\frac{\Delta}{\sqrt{\xi_1^2+\Delta^2}}\right)\right|_{\Delta_c}, \quad (59)$$

because of the following reason: At $T=0$, this term has nonzero value only at $E_\eta(\mathbf{k},\Delta)=0$ (on the Fermi surface) because $\partial f(E_\eta(\mathbf{k},\Delta))/\partial\Delta$ becomes the δ function. At the MI transition point, since the Fermi energy has the same value as that of the top [bottom] of the lower [upper] band, $\partial f(E_-(\mathbf{k},\Delta))/\partial\Delta$ [$\partial f(E_+(\mathbf{k},\Delta))/\partial\Delta$] has nonzero value only at $(\pi/2,\pi/2)$ [$(\pi,0)$], respectively. However, at the MI transition point—namely, at $(\pi/2,\pi/2)$ and $(\pi,0)$—$\xi_1=0$ is satisfied; then, $\partial/\partial\Delta(\Delta/\sqrt{\xi_1^2+\Delta^2})$ becomes zero. From this, the term defined in Eq. (59) vanishes at the MI transition point $\Delta=\Delta_c$ at $T=0$.

Next, we derive more explicit forms of the coefficients B and C at $T=0$. We first consider the contribution of the first term of Eqs. (53) and (54) at $T=0$. The first term of Eq. (53) is given by

$$\frac{1}{N_s}\sum_{\mathbf{k},\eta}\left.\left(\frac{\partial f(E_\eta(\mathbf{k},\Delta))}{\partial\Delta}\frac{\Delta}{\eta\sqrt{\xi_1^2+\Delta^2}}\right)\right|_{\Delta_c} = -\sum_\eta\int_{-\Lambda}^{\Lambda} dE\, D_\eta(E_\eta)G(T,E_\eta)\times\left(\frac{\Delta_c}{\eta\sqrt{\xi_1^2+\Delta_c^2}}+\tilde{\alpha}\right)\left(\frac{\Delta_c}{\eta\sqrt{\xi_1^2+\Delta_c^2}}\right), \quad (60)$$

where D_η (E_η) is the density of states of the upper (lower) band for $\eta=+1$ (-1), respectively, Λ is a cutoff, and $G(T,E)$ is defined by

$$G(T,E) = \frac{\exp(E/T)}{T[1+\exp(E/T)]^2}. \quad (61)$$

We introduce a constant $\tilde{\alpha}$ for the linear coefficient between $\Delta_c-\Delta$ and μ as

$$\mu = \tilde{\alpha}(\Delta_c-\Delta) - 2t'. \quad (62)$$

A detailed derivation of $\tilde{\alpha}$ at $T=0$ is described in Appendix B. The explicit form of $\tilde{\alpha}$ at $T=0$ is given by

$$\tilde{\alpha} = \frac{2t'-\sqrt{t^2-t'^2}}{2t'+\sqrt{t^2-t'^2}}. \quad (63)$$

The function $G(T,E)$ becomes the δ function at $T=0$. Then, Eq. (60) is discontinuous at the MI transition at $T=0$, because the density of states at the Fermi level is discontinuous between the metallic and insulating sides. In fact, at $T=0$, we obtain the relation

$$(60) := \begin{cases} -[D_+(1+\tilde{\alpha}) + D_-(1-\tilde{\alpha})] & \text{for } Y>0, \\ 0 & \text{for } Y<0, \end{cases}$$

where D_+ (D_-) is the density of states at the bottom (top) of the upper (lower) band, respectively. Explicit forms of D_+ and D_- are given by

$$D_+ = \frac{1}{4\pi t'}, \quad (64)$$

$$D_- = \frac{1}{2\pi\sqrt{t^2-t'^2}}. \quad (65)$$

Detailed derivations of D_+ and D_- are given in Appendix B.

Using a similar derivation, we obtain the representation of the first term of Eq. (54) as

$$-\sum_\eta\int_{-\Lambda}^{\Lambda} dE\, D_\eta(E_\eta)\frac{\partial G(T,E_\eta)}{\partial\Delta}\times\left(\frac{\Delta_c}{\eta\sqrt{\xi_1^2+\Delta_c^2}}+\tilde{\alpha}\right)^2\left(\frac{\Delta_c}{\eta\sqrt{\xi_1^2+\Delta_c^2}}\right). \quad (66)$$

From this, we obtain the relation as

$$(66) := \begin{cases} -(1+\tilde{\alpha})^2 R_+(T) + (1-\tilde{\alpha})^2 R_-(T) + \dfrac{Q_+(T)}{\Delta_c}(1+\tilde{\alpha})(3+\tilde{\alpha}) + \dfrac{Q_-(T)}{\Delta_c}(1-\tilde{\alpha})(3-\tilde{\alpha}) & \text{for } Y>0, \\ 0 & \text{for } Y<0, \end{cases}$$

where $R_\pm(T)$ and $Q_\pm(T)$ are defined by

$$R_\eta(T) = \int_{-\Lambda}^{\Lambda} dE_\eta \frac{\partial D_\eta(E_\eta)}{\partial E_\eta} G(T,E_\eta), \tag{67}$$

$$Q_\eta(T) = \int_{-\Lambda}^{\Lambda} dE_\eta \frac{D_\eta(E_\eta)^2}{D_\eta(\sqrt{\xi_1^2+\Delta^2})} G(T,E_\eta). \tag{68}$$

Finally, at $T=0$, we obtain the free-energy expansion for metallic and insulating sides as

$$F = AY + \frac{B_m}{2!}Y^2 + \frac{C_m}{3!}Y^3 + \cdots, \tag{69}$$

$$F = AY + \frac{B_i}{2!}Y^2 + \frac{C_i}{3!}Y^3 + \cdots, \tag{70}$$

where

$$A = -\left(\frac{1}{g} - W_1\right)\Delta_c \tag{71}$$

and the coefficients of the metallic side ($\Delta<\Delta_c$) are given as

$$B_m = -W_2 - [(1+\tilde{\alpha})D_u + (1-\tilde{\alpha})D_l] + \frac{1}{g}, \tag{72}$$

$$C_m = -3W_3 - R_+(0)(1+\tilde{\alpha})^2 + R_-(0)(1-\tilde{\alpha})^2 + \frac{Q_+(0)}{\Delta_c}(1+\tilde{\alpha}) \times(3+\tilde{\alpha}) + \frac{Q_-(0)}{\Delta_c}(1-\tilde{\alpha})(3-\tilde{\alpha}), \tag{73}$$

and the coefficients of the insulating side ($\Delta>\Delta_c$) are given as

$$B_i = -W_2 + \frac{1}{g}, \tag{74}$$

$$C_i = -3W_3. \tag{75}$$

We emphasize that, while A is common, the coefficients B and C in the region $Y>0$ have values different from those in the region $Y<0$ at $T=0$. Although the coefficients B and C jump at $Y=0$, F is regular (namely, piecewise analytic) within each region $Y>0$ and $Y<0$. Then the Taylor series expansion (69) as well as (70) is allowed in each sector $Y>0$ and $Y<0$ separately and they are unique. The coefficient C_i is negative if t' is not too large, because the sign of W_3 is determined from the dominant contribution proportional to v_3, which has a positive sign due to the contribution from the lower band dominating over the upper-band contribution. On the other hand, C_m is positive for the relevant region of t'—namely, for not too large value of $|t'|$—because the dominant contribution is then from the term proportional to Q_+. Therefore, the MI transition takes place in the parameter regions of $C_m>0$ and $C_i<0$, which makes F always bounded from below within the expansion up to the cubic order of Y. In fact, we will show below that the expansion up to cubic order is enough for the purpose of deriving critical properties. Note that this expansion up to cubic order is consistent with that obtained in the scaling theory and its phenomenological extension for two-dimensional systems.[39–41] We will show below that the universality class obtained in the present paper by the microscopic Hartree-Fock calculation indeed agrees with the prediction of the scaling theory and further reveals a microscopic mechanism of the emergence of the unconventional universality.

The carrier density X, which is the sum of the electron density X_- and the hole density X_+ in the metallic phase near MI transitions, is given as

$$X = X_+ + X_- = \frac{1}{\pi\Delta_c}(1+\tilde{\alpha})Y. \tag{76}$$

Details of the derivation of Eq. (76) are given in Appendix A. Since X is proportional to Y in the metallic phase, the singularity of X is the same as that of Y. Therefore, whichever of X or Y is taken as the order parameter, the critical exponents are the same in the metallic side.

B. Critical exponents

Using the free-energy expansion obtained in the previous subsection, we are able to obtain the critical exponents of the quantum MI transitions.

The phase diagram of the MI transitions in the $A-B_m$ plane is shown in Fig. 4 for the region close to $A=B_m=0$. Metallic states are realized when the minimum is at a positive Y_m, whereas insulating states are stabilized when the minimum is at a negative Y_i. From Eq. (51), a local minimum appears at

$$Y_m = \frac{-B_m + \sqrt{B_m^2 - 2AC_m}}{C_m}, \tag{77}$$

if $B_m^2>2AC_m$, and at

$$Y_i = \frac{-B_i + \sqrt{B_i^2 - 2AC_i}}{C_i}, \tag{78}$$

if $B_i^2>2AC_i$ is satisfied. Because F is bounded from below, there always exists the absolute minimum in either the region $Y_i\leqslant 0$ or $Y_m\geqslant 0$. The location of the absolute minimum and the phase boundary shown in Fig. 4 are clarified below by

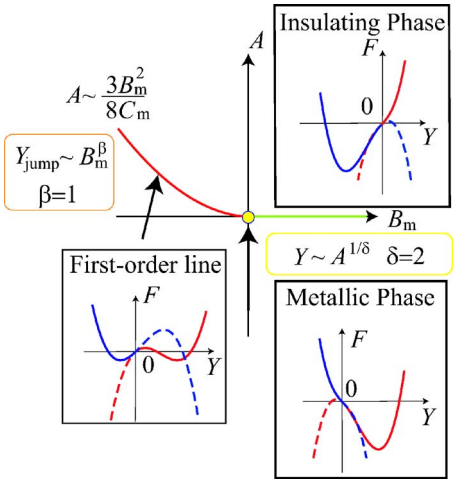

FIG. 4. (Color online) Phase diagram in the $A-B_m$ plane. The first-order transition line is given by the condition $A\sim 3B_m^2/8C_m$ with $B_m<0$, which separates the metallic phase $A<3B_m^2/8C_m$ from the insulating phase in the other side. For $B_m>0$ the transition becomes continuous and the transition line is given by $A=0$ [see Eq. (95)]. Typical Y dependence of the free energy along the first-order transition line, in the metallic and insulating phases, is also shown in the insets. The definition of the free energy is given in Eqs. (69) and (70). The real Y dependence of the free energy is represented by the solid lines, where the metallic (insulating) side corresponds to the region $Y>0$ ($Y<0$), respectively. Deshed lines represent the behaviors of Eqs. (69) and (70) extrapolated to the other sides $Y<0$ and $Y>0$, respectively. For the derivation of the phase boundary, see the text.

classifying the parameter values into several cases. Then the critical exponents are derived in each region. We recall that $B_i>B_m$ and $C_i<0<C_m$ are always satisfied in all relevant regions.

1. Quantum critical line

The continuous MI transition line (quantum critical line) is determined from the condition $A=0$ and $B_m>0$. Along this quantum critical line, the free-energy minimum exists at $Y=0$. For nonzero A near the quantum critical line $A=0$, Eqs. (77) and (78) are reduced to

$$Y_m \sim -\frac{A}{B_m} \tag{79}$$

and

$$Y_i \sim -\frac{A}{B_i}, \tag{80}$$

respectively. Because the coefficient A plays the role of the conjugate field to Y, the critical exponent δ is defined from the growth of Y for small but nonzero A as

$$Y \sim A^{1/\delta}. \tag{81}$$

Therefore, $\delta=1$ is obtained in both the metallic and insulating sides.

The susceptibility in the metallic and insulating phases is given by

$$\chi = \left(\frac{d^2F}{d(Y)^2}\right)^{-1} \sim \frac{1}{B_m},$$

$$\chi = \left(\frac{d^2F}{d(Y)^2}\right)^{-1} \sim \frac{1}{B_i}, \tag{82}$$

respectively. Along the quantum critical line, B is of course always positive for the region $B_m>0$ in whichever of the insulating and metallic sides. Therefore, the susceptibility does not diverge and the critical exponent defined by

$$\chi \sim A^{-\gamma} \tag{83}$$

is given as

$$\gamma = 0. \tag{84}$$

As we showed in Eq. (14) in Sec. I, the critical exponent α does not represent the singularity of the specific heat in the case of the quantum phase transition. It rather characterizes the singularity of $\chi=\partial^2 F/\partial A^2$, because in the present case around the quantum critical line, $A\propto g-g_c$ holds. Near the quantum critical line of the MI transition, the free energy F at the minimum is scaled by A as

$$F \propto A^2, \tag{85}$$

as is shown by substituting Eqs. (79) and (80) into Eqs. (69) and (70). From Eq. (14), this indicates $\alpha=0$. The exponent β is not well defined on the quantum critical line,[50] because it is not possible to control the parameter g to cause the phase transition without applying the field A conjugate to the order parameter.

The free-energy form (69) and (70) with nonzero A, B_i, and B_m is equivalent to the case of the transition between metals and band insulators for noninteracting electron systems if one replaces Y with the carrier density X of noninteracting electrons. By utilizing the equivalence with this noninteracting system, in the present case of the quantum critical line, we also obtain $\xi\propto X^{-1/2}\propto|g-g_c|^{-1/2}$, leading to $\nu=1/2$. On the other hand, one can also calculate the dynamical susceptibility χ of the carrier density in the noninteracting system, which yields $\chi/S\propto E_F^{-1}\propto k_F^{-2}\propto\xi^2$. Here, E_F is the Fermi energy. This leads to the dynamical exponent $z=2$.

Now we summarize the critical exponents on the quantum critical line: $\alpha=0$, $\gamma=0$, $\delta=1$, $\nu=1/2$, and $z=2$. This is common to both the insulating and metallic sides of the transition.

2. Marginal quantum critical point

When B_m becomes zero, the quantum critical line terminates at the *marginal quantum critical point* and the first-order transition boundary starts. Around MQCP, we show that the exponents depend on the approach to the critical point either from the metallic side or from the insulating side. To clarify such a route dependence, we introduce four routes to approach the MQCP as is illustrated in Fig. 5.

From the free-energy expansion, the coefficient A represents the conjugate field to the order parameter and B represents the control parameter g. Therefore, we obtain the critical exponent δ through the route (a) or (b) in the following:

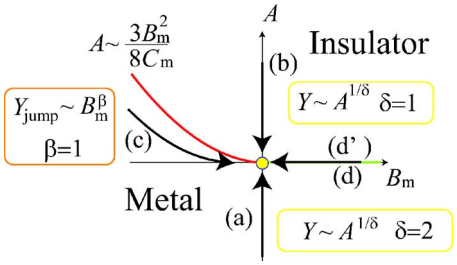

FIG. 5. (Color online) Four routes to approach the MQCP. The solid line in the negative B_m region represents the first-order transition line. The quantum critical line is given by the condition $A=0$ and $B_m>0$ (see text). Route (a) is the way to approach the MQCP by controlling the "external field" A from the metallic region. The singularity of Y along the route (a) is characterized by the critical exponent δ. Route (b) is the way to approach the MQCP from the insulating phase. Route (c) is the way to approach the MQCP along the first-order transition line $A \sim \frac{3}{8}B_m^2$ as is derived in Eq. (96). Route (d) $[(d')]$ is the way to approach the MQCP along the quantum critical line from the metallic [insulating] phase.

Route (a). In the metallic side, through route (a) in Fig. 5, the coefficient A approaches zero by keeping $B_m=0$. From Eq. (77), neglecting B_m, we obtain the singularity of Y as

$$Y_m \propto \sqrt{\frac{2|A|}{C_m}} \propto |A|^{1/2}. \tag{86}$$

Therefore, the critical exponent δ in the metallic side is

$$\delta = 2. \tag{87}$$

Note that this exponent is consistent with the value obtained in the scaling theory[2,3,39–41] as well as with that in quantum Monte Carlo studies.[29–31]

The dynamical exponent of the present transition can be calculated from the correlation functions of the order parameter X. Namely, from the equal-time structure factor S for the carrier density X defined in Eq. (34) and the susceptibility χ defined in Eq. (35), z is given by Eq. (6). By calculating S and χ, we obtain $z=4$.[51] Alternatively, we can derive z from the following arguments: The characteristic length scale of the MI transitions is given by the mean carrier distance ξ, which diverges at the continuous MI transition point including the MQCP. Then, in two dimensions, the carrier density X is proportional to ξ^{-2}. The equal-time structure factor S has the same scaling $\propto \xi^2$ by definition. On the other hand, from $\delta=2$, the susceptibility of the carrier density χ is scaled by $X^{-1} \propto \xi^{-2}$. Then the dynamical critical exponent z is determined from the condition

$$\frac{\chi}{S} \propto \xi^z, \tag{88}$$

as $z=4$. It also yields that ξ has the singularity $\xi \propto |g-g_c|^{-\nu}$ with $\nu=1/2$. The large dynamical exponent $z=4$ is consistent with the previous predictions obtained beyond the mean-field approximations.[2,3,30,31]

The origin of such an unusually large z is now clarified from the present study: The dynamical exponent normally expresses the dispersion of quantum dynamics. Namely, one might expect that the carrier dynamics would be described by the dispersion $\epsilon \propto k^4$. However, this contradicts the quasiparticle dispersion (44), which is generically proportional to k^2. This puzzle is solved when we realize that the gap amplitude decreases with the increase of carrier number. Because of this reduction of the gap, when the carrier density is fixed, the upper (lower) band edge as well as the Fermi level becomes lower (higher) than that we might expect from the rigid-band picture obtained from the quasiparticle dispersion of insulators. Because of this self-consistent reduction of the gap, the Fermi level does not move as quickly as k^2 with increasing X and is rather pinned near the original band edge even when the carrier number increases. This results in an effectively flat dispersion and actually a higher exponent with $z=4$ comes out. This is an intuitive picture for the filling-control transition. For the case of bandwidth control, where the chemical potential is fixed rather than the filling, the reduction of the gap further allows more electrons and hole carriers, which is again interpreted by an effectively flatter dispersion.

Routes (b) and (d'). In the insulating phase, through routes (b) and (d') in Fig. 5, only A becomes zero while B_i remains nonzero and positive even at the MQCP. This condition generates the same criticality as that of the quantum critical line. Therefore, we obtain the critical exponents $\alpha=0$, $\delta=1$, $\gamma=0$, and $z=2$.

Route (c). Next we consider the critical exponent β defined by

$$Y_{jump} \sim |B_m|^{\beta}, \tag{89}$$

where Y_{jump} is the jump of Y across the first-order transition line located in the region $B_m<0$. Near the MQCP, from Eqs. (77) and (78), Y_{jump} is given by

$$Y_{jump} \equiv Y_m - Y_i \sim \frac{|B_m|\lambda}{C_m} + \frac{A}{B_i}, \tag{90}$$

where we define $\lambda \equiv 1+\sqrt{B_m^2-2AC_m}/|B_m|$. From this definition, it turns out that λ is of order unity. On the first-order transition line, the free energy in the metallic phase has the same value as that of the insulating phase—namely,

$$F(Y_m) = F(Y_i). \tag{91}$$

Equation (91) leads to

$$\frac{A\lambda|B_m|}{C_m} + \frac{B_m(\lambda|B_m|)^2}{2C_m^2} + \frac{C_m(\lambda|B_m|)^3}{6C_m^3} = -\frac{A^2}{2B_i^2}. \tag{92}$$

Near the MQCP, $|C_m|$ and $|B_i|$ are always nonzero and have amplitudes of order unity. We assume that, for small quantities A and B_m, A has the order ϵ_1 and B_m has the order ϵ_2. From Eq. (92), the relation between ϵ_1 and ϵ_2 is given by

$$O(\epsilon_1)O(\epsilon_2) + O(\epsilon_2^3) \sim O(\epsilon_1^2). \tag{93}$$

From this, to satisfy Eq. (92), the relation between ϵ_1 and ϵ_2 should be

$$\epsilon_1 \sim \epsilon_2^2. \tag{94}$$

Substituting Eq. (92) into Eq. (77) leads to $\lambda=3/2$. Namely, on the first-order transition line near MQCP, the relation between A and B_m should be

$$A \sim \frac{3B_m^2}{8C_m}. \tag{95}$$

Using this relation, near the MQCP, the singularity of Y_{jump} is given by

$$Y_{jump} \sim \frac{3B_m^2}{8C_m B_i} + \frac{3|B_m|}{2C_m} \propto |B_m|. \tag{96}$$

Therefore, the critical exponent β is given by

$$\beta = 1. \tag{97}$$

Route (d). Route (d) along the quantum critical line ($A=0$ and $B_m>0$) always keeps $A=0$. Although the susceptibility χ remains finite on the quantum critical line itself ($\chi=1/B_m$), the amplitude $1/B_m$ increases toward the MQCP and it diverges in the limit to the MQCP because of $B_m \to 0$. The singularity of the susceptibility,

$$\chi = |g - g_c|^{-\gamma}, \tag{98}$$

is given by

$$\chi = \left(\frac{d^2F}{d(Y)^2}\right)^{-1} \propto |B_m|^{-1} \propto |g - g_c|^{-1}. \tag{99}$$

Therefore, in the metallic phase, the susceptibility diverges at the MQCP with the critical exponent

$$\gamma = 1. \tag{100}$$

Near the MQCP, the free energy F at the minimum in the metallic side is scaled by the control parameter B_m as

$$F \propto B_m^3. \tag{101}$$

For the MQCP, $B_m \propto g - g_c$ holds in contrast to $A \propto g - g_c$ for the quantum critical line. Then, from Eq. (14), we obtain the exponent $\alpha=-1$. We remark again that α has no direct relation to the singularity of the specific heat. In the insulating side, as mentioned above for the route (d'), $\alpha=0$ is obtained.

Now the critical exponents for the MQCP are summarized as

$$\alpha = -1, \quad \beta = 1, \quad \gamma = 1, \quad \delta = 2, \quad \nu = 1/2, \quad z = 4 \tag{102}$$

for the metallic side and

$$\alpha = 0, \quad \beta = 1, \quad \gamma = 0, \quad \delta = 1, \quad \nu = 1/2, \quad z = 2 \tag{103}$$

for the insulating side. The scaling laws (15) and (16) as well as the hyperscaling Josephson relation (24) associated with the hyperscaling equation (9) are all satisfied in both sides.

C. Crossover of the critical exponent δ

In the metallic region, Y grows from zero at MQCP when A and/or B_m deviate from zero. As a function of the distance from the MQCP defined by $r=\sqrt{A^2+B_m^2}$ in the $A-B_m$ plane, Y grows as $Y \propto r$ for $A=0$ because of Eq. (96) whereas it is scaled as $Y \propto r^{1/2}$ for $B_m=0$ because of Eq. (86). Then a crossover between $Y \propto r$ and $Y \propto r^{1/2}$ must exist. Here, we specify the location of this crossover boundary below.

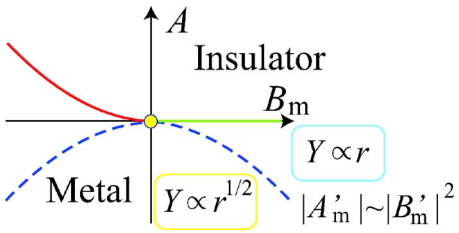

FIG. 6. (Color online) Crossover line between the scaling region $Y \propto r$ and $Y \propto r^{1/2}$, which is represented by the dashed (blue) line defined by $A' \sim |B'_m|^2$.

Near the MQCP, Y_m is given as

$$Y_m \sim \frac{-B_m + \sqrt{B_m^2 - 2AC_m}}{C_m} \tag{104}$$

$$= -B'_m + \sqrt{B'^2_m + A'_m}, \tag{105}$$

where we define $B'_m = B_m/C_m$ and $A'_m = -2A/C_m > 0$. In the region where the condition $A'_m \gg B'^2_m$ is satisfied, Y_m behaves as

$$Y_m \sim -B'_m + \sqrt{A'_m} \propto A^{1/2}. \tag{106}$$

This indicates that the MQCP exponent ($\delta=2$) dominates in this region. In contrast, in the region where the condition $A'_m \ll B'^2_m$ is satisfied, Y_m behaves as

$$Y_m \sim -B'_m + B'_m\left(1 + \frac{A'_m}{B'^2_m}\right) \tag{107}$$

$$\sim \frac{A'_m}{B'_m} \propto |A|. \tag{108}$$

From this, in this region the criticality of the quantum critical line represented by $\delta=1$ dominates. In Fig. 6, the crossover line is represented by the dashed line.

D. Location of the marginal quantum critical point

From the free-energy form, the location of the MQCP is determined by the condition

$$A = 0 \quad \text{and } B_m = 0. \tag{109}$$

The line $A=0$ is determined by

$$\Delta = \Delta_c, \tag{110}$$

with the definition $\Delta_c = 2t'$. From Eq. (110), the relation between g and t' for $A=0$ is given, because Δ is an implicit function of g and t'. We calculate B_m from Eq. (72) with the condition (110). We then find that B_m becomes zero at two points; namely, two MQCP's exist at zero temperature. Figure 7 shows the numerical estimate of B_m near the MQCP from Eq. (72).

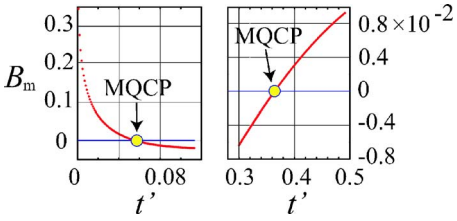

FIG. 7. (Color online) Coefficient B_m on the line $A=0(\Delta=\Delta_c)$ near the MQCP. We estimate the points $B_m=0$ as $t'/t=0.05571$ and 0.36455. In the positive-B_m region, the continuous MI transition occurs, while in the negative-B_m region, the first-order MI transition occurs.

From this, we estimate the location of the MQCP at $t_c'/t=0.055\,71$, $g_c=0.616\,180$ and $t_c'/t=0.364\,55$, $g_c/t=1.381\,44$, respectively. We call the MQCP at $t_c'=0.055\,71$ MQCP_1 and the MQCP at $t_c'=0.364\,55$ MQCP_2, respectively.

E. Finite-temperature effect

In this subsection, we analyze how the free energy and critical properties are modified at nonzero temperatures. Since the discontinuity of the coefficient arising from the singularity of the density of states is immediately smeared out by the Fermi distribution at $T>0$, the free-energy expansion should convert into an expansion of the conventional ϕ^4 theory in the critical region. The universality class of the MQCP then switches over to the Ising universality class. Here, we show how the expansion in Eq. (51) breaks down and the Ising critical region appears.

The discontinuity of the coefficient B and C comes from integration of the form

$$P=\int_{-\Lambda}^{\Lambda} dE \sum_{\eta=\pm} D_\eta(E)H(E)G(T,E), \tag{111}$$

where $H(E)$ is a slowly varying function of E in the range $E\sim O(T)$. Now the density of states, $D_+(E)$, is nonzero only in the interval

$$-(1-\tilde{\alpha})Y<E<\Lambda, \tag{112}$$

whereas $D_-(E)$ is nonzero in the window

$$-\Lambda<E<(1+\tilde{\alpha})Y. \tag{113}$$

The correction factor proportional to $\tilde{\alpha}$ arises from the chemical potential shift from the case of $Y=0$. By considering Eq. (61), Eq. (111) is reduced to

$$P\cong 2H(0)\sum_{\eta} D_\eta\left(1+\tanh\frac{(1-\eta\tilde{\alpha})Y}{2T}\right) \tag{114}$$

if the energy dependence of the density of states, $D_\eta(E)$, can be ignored. Since $(1-\tilde{\alpha})/2$ and $(1+\tilde{\alpha})/2$ in Eq. (114) are the quantities of the order unity, from Eq. (111), for $Y\gg T$, P behaves similarly to that of the step function as shown in Fig. 8. Therefore, for $Y\gg T$, the expansion (51) is valid and the MQCP criticality appears. We call this region the quantum region. On the other hand, for $Y\ll T$, P behaves differently from that of the step function as shown in Fig. 8 and behaves as a smooth function of Y. Therefore, the expansion (51) breaks down and the conventional GLW expansion (3) becomes justified, where the Ising criticality appears. We call this region the classical region. We expect that fluctuations modify the mean-field exponents for the Ising universality because the upper critical dimension of the Ising universality is 4. We do not go into detail on this point.

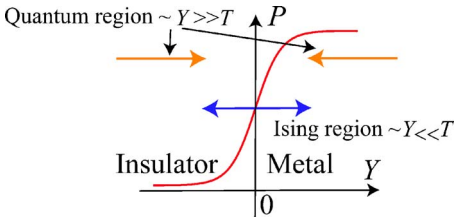

FIG. 8. (Color online) Schematic behavior of P as a function of Y. In the $Y\gg T$ region P behaves as a step function and the expansion (51) is valid, while in the $Y\ll T$ region P behaves as a Fermi distribution function and the expansion (51) breaks down.

Now, we clarify the width of the quantum region for each route shown in Fig. 9.

Route (*a*). In the quantum region, the singularity of Y_m is given from Eq. (86) as

$$Y_m\propto\sqrt{\frac{|A|}{C_m}}\sim a|g-g_c|^{1/2}, \tag{115}$$

where a is a g-independent constant given by

$$a=\lim_{|g-g_c|\to 0}\frac{1}{|g-g_c|^{1/2}}\sqrt{\frac{|A|}{C_m}}. \tag{116}$$

From this, the condition of the quantum region $Y\gg T$ is given by

$$|g-g_c|\gg\frac{T^2}{a^2}. \tag{117}$$

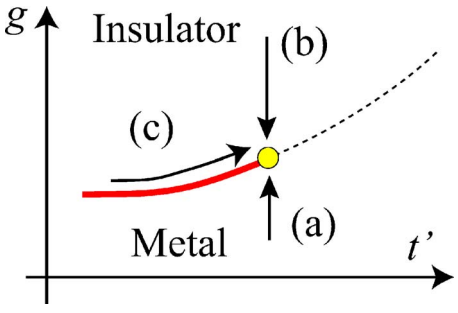

FIG. 9. (Color online) Routes to the critical point in the plane of g and t' at fixed temperature T. The solid thick (red) line represents the first-order transition line and it terminates at the finite-temperature critical point represented by the (yellow) circle. Route (c) is the way to the finite-temperature critical point along the first-order transition line with constant T. Routes (a) and (b) are the routes to the critical point with fixed temperature from the metallic and insulating phases, respectively. The dashed line represents the crossover line, where $|d\Delta/dg|$ has the maximum value.

Route (b). In the quantum region, the singularity of Y_i is given by

$$Y_i \propto \frac{A}{B_i} \sim b|g - g_c|, \tag{118}$$

where b is a g-independent constant defined by

$$b = \lim_{|g-g_c|\to 0} \frac{1}{|g-g_c|}\frac{A}{B_i}. \tag{119}$$

From this, the condition of the quantum region $Y \gg T$ is given by

$$|g - g_c| \gg \frac{T}{b}. \tag{120}$$

Route (c). In the quantum region, the singularity of Y_{jump} is given from Eq. (96) as

$$Y_{jump} \propto \frac{|B_m|}{C_m} \sim c|t' - t'_c|, \tag{121}$$

where a g-independent constant c is defined by

$$c = \lim_{|t'-t'_c|\to 0} \frac{1}{|t'-t'_c|}\frac{B_m}{C_m}. \tag{122}$$

From this, the condition of the quantum region $Y \gg T$ is given by

$$|t' - t'_c| \gg \frac{T}{c}. \tag{123}$$

IV. NUMERICAL HARTREE-FOCK RESULTS AT $T=0$

In this section, we show numerical results of the MQCP obtained by numerically solving the Hartree-Fock self-consistent equation (46) itself without relying on the free-energy expansion (51). We will show that numerical results are consistent with the free-energy expansion in the previous section.

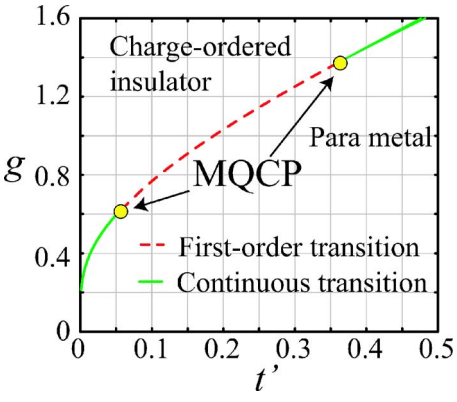

FIG. 10. (Color online) Phase diagram at $T=0$. The dashed (solid) line represents the first-order (continuous) transition line, respectively. Near the MQCP, charge-ordered metal appears. The detailed phase diagram near the MQCP is shown in Figs. 11(a) and 11(b)

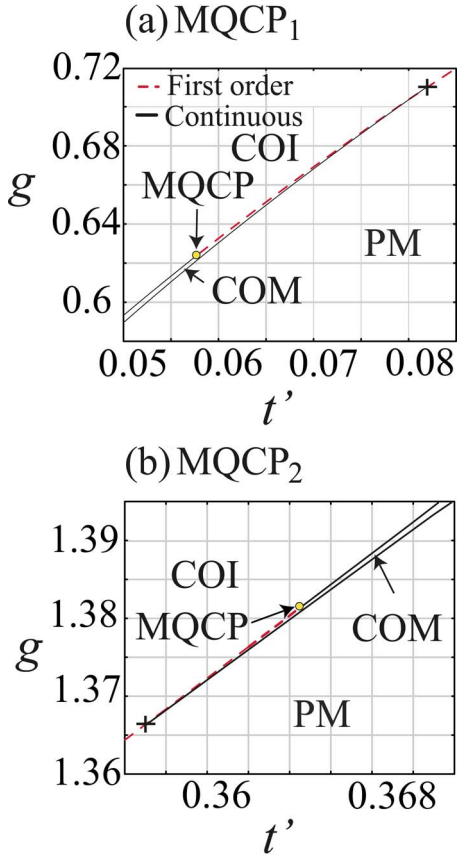

FIG. 11. (Color online) (a) Phase diagram near $MQCP_1$ ($t' \sim 0.05571t, g \sim 0.6161t$). The continuous (first-order) transition is shown by the solid (dashed) line, respectively. The MQCP is shown by the circle, where the first-order transition line terminates. The cross point represents the triple point where COI, COM, and PM coexist. (b) Phase diagram near $MQCP_2$ ($t' \sim 0.3645t$, $g \sim 1.381t$).

A. Phase diagram at zero temperature

We first present the phase diagram at $T=0$ in Fig. 10. We find two MQCP's in the phase diagram in agreement with the free-energy expansion.

At $t'=0$, perfect nesting occurs and the charge-ordered phase begins from $g=0$. For a narrow window below the triple point ($t' \sim 0.085t, g \sim 0.694t$), charge-ordered metal (COM) appears between paramagnetic-metal (PM) and charge-ordered insulator (COI) phases as is shown in Fig. 11(a) in detail. The triple point represents the point where PM, COM, and COI coexist. The order of the transitions from PM to COM is continuous, while the order of transition from COM to COI changes from continuous to first order with increasing t'/t. The continuous transition line between PM and COM terminates at the triple point. The quantum critical line between COI and COM terminates at $MQCP_1$ ($t' \sim 0.055\,71t, g \sim 0.6161t$).

For the large-t' region ($t' > 0.35t$), another triple point appears at $t' \sim 0.357t$, $g \sim 1.366t$ and COM appears between COI and PM as is shown in Fig. 11(b) in detail. The quantum critical line between COM and COI terminates at $MQCP_2 (t' \sim 0.3645t, g \sim 1.381t)$ again.

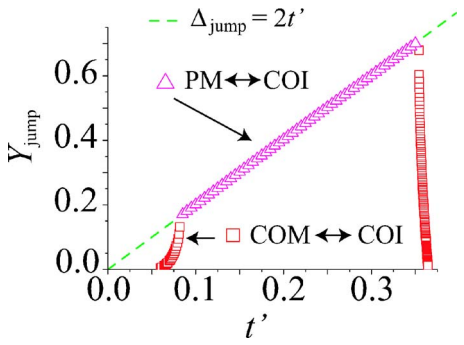

FIG. 12. (Color online) Y_{jump} as a function of t' on the first-order MI transition line. For the first-order transition between PM and COI shown by triangles, Y_{jump} is slightly larger than $\Delta_c=2t'$.

Figure 12 shows the jump of Y (Y_{jump}) as a function of t' across the first-order MI transition line at $T=0$. The (red) squares and (purple) triangles show Y_{jump} between COM and COI and between COI and PM, respectively, as a function of t'. Y_{jump} vanishes at MQCP.

B. Critical exponents of MQCP

We clarify the singularity of Y near the MQCP numerically. Hereafter, we only consider the MQCP at $t_c'=0.364\,55$—namely, $MQCP_2$ through routes (a)–(d) in Fig. 5. The critical exponents of $MQCP_1$ are the same as that of $MQCP_2$. We show that the numerical Hartree-Fock results are consistent with the results obtained by the free-energy expansion in the previous section.

Route (*a*). First, we confirm that the critical exponent δ in the metallic region, defined by

$$Y_m \propto |A|^{1/\delta}, \quad Y_m \sim a|g-g_c|^{1/\delta}, \tag{124}$$

is consistent with the value obtained by the free-energy expansion. We perform a least-squares fitting for Y_m as a function of g_c-g near the MQCP. Figure 13 shows the results of

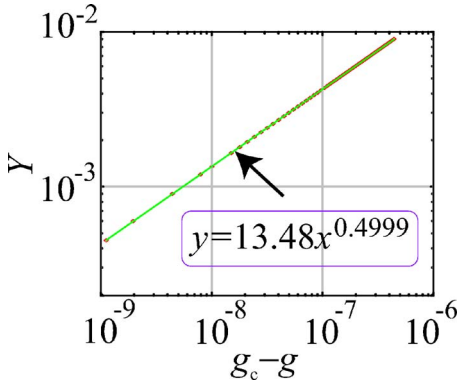

FIG. 13. (Color online) Log-log plot of Y_m as a function of g_c-g at $t'/t=0.36455$. The solid (green) line shows the result of a least-squares fitting by assuming the function $y=ax^{1/\delta}$, where $y=Y_m$ and $x=(g_c-g)$. The results of the least-squares fitting are given as $1/\delta=0.49996(2)$ and $a=13.48(4)$. The critical gap Δ_c is obtained as $\Delta_c=2t'=0.72911t$, and the critical interaction g_c is estimated as $g_c=1.38144$.

the least-squares fitting. We estimate the critical exponent δ as

$$\delta = 2.0001(6). \tag{125}$$

This is consistent with $\delta=2$ obtained by the free-energy expansion. We estimate the coefficient a defined in Eq. (116) as

$$a = 13.48(4). \tag{126}$$

Route (*b*). We also obtain the critical exponent δ in the insulating region. The definition of δ is given by

$$Y_i \propto |A|^{1/\delta}, \quad Y_m \sim b|g-g_c|^{1/\delta}. \tag{127}$$

The numerically obtained critical exponent δ is

$$\delta = 1.000\,000(4). \tag{128}$$

The coefficient b defined in Eq. (119) is estimated as

$$b = 0.996\,429(4). \tag{129}$$

Now it was confirmed that the Hartree-Fock result is consistent with the exponent $\delta=1$ obtained by the free-energy expansion.

Route (*c*). Next, we consider the critical exponent β defined by

$$Y_{jump} \propto |B_m|^{\beta} \propto c|t'-t_c'|^{\beta}. \tag{130}$$

We estimate the critical exponent β as

$$\beta = 1.01(1). \tag{131}$$

This critical exponent is consistent with $\beta=1$ obtained by the free-energy expansion. The coefficient c defined in Eq. (122) is estimated as

$$c = 35.2(1). \tag{132}$$

C. Crossover of the critical exponent δ

The critical exponent δ has different values between the quantum critical line and MQCP, and it may show a crossover when the critical regions meet. Here, we show numerical results for the crossover of the critical exponent δ at $T=0$. As already mentioned, at the MQCP, the singularity of Y is well fit by the function $a|g-g_c|^{1/\delta}$ with $\delta=2$ and $a=13.48$. Away from the MQCP, δ crosses over from 2 to 1 near the quantum critical line. In Fig. 14, we show the least-squares fitting for the g_c-g dependence of Y by assuming the function $a'|g-g_c|^{1/\delta}$, where $\delta=1$. The crossover point is estimated by the crossing point of the function $a|g-g_c|^{1/2}$ and $a'|g-g_c|$, which is illustrated in Fig. 15. The inset of Fig. 15 shows that the t' dependence of the crossover point is well fit by the function $|t'-t_2'|^2$. This is consistent with the analytical result.

V. NUMERICAL HARTREE-FOCK RESULTS AT $T\neq 0$

To understand quantitatively, we numerically study how the critical exponents of the MQCP cross over to those of the Ising critical points by finite-temperature effects. As shown in the previous section, the free-energy expansion predicts

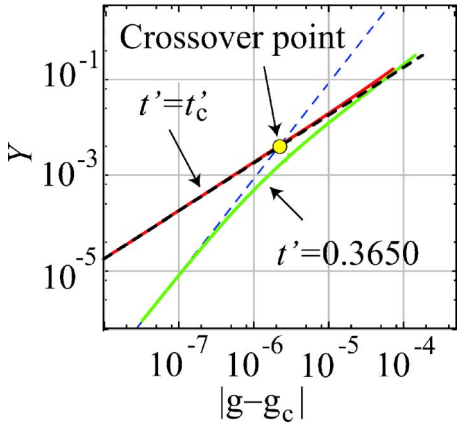

FIG. 14. (Color online) Crossover points of the critical exponent δ determined from the $g-g_c$ dependence of Y for $t'=0.3650$ near $MQCP_2$ at $t'=0.364555$. Away from the transition point, the behavior of Y for $t'=0.3650$ asymptotically approaches that of Y for $t'=0.364555$. The crossover point is determined from the crossing point of $a|g-g_c|^{1/2}$ and $a'|g-g_c|$. The t' dependence of the crossover point is shown in Fig. 15.

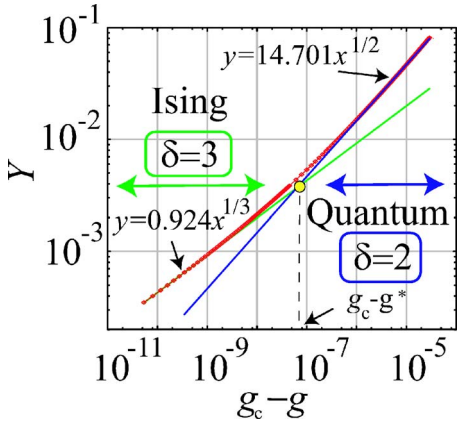

FIG. 16. (Color online) Log-log plot of Y_m as a function of $|g-g_c|$ near the critical point at $T=0.001t$. Two thin solid (green and blue) lines show the results of a least-squares fitting by assuming the functions $y=ax^{1/3}$ and $y=a'x^{1/2}$, respectively, where $y=Y_m$ and $x=g-g_c$. We obtain $a=0.924(1)$ and $a'=14.701(3)$.

that crossovers of the critical exponents depend on routes (a)–(c).

Route (*a*). In the metallic phase, we show the crossover of the critical exponent δ near the critical point for an example of $T=0.001t$ in Fig. 16. Here, δ clearly crosses over from 2 (MQCP) to 3 (Ising mean-field value). We estimate the width of the Ising region by the crossing point of two solid (green and blue) asymptotic lines. The value of g at the crossing point is denoted as g^*. The Ising region is given by $W<W^*$ for

$$W \equiv |g_c - g| \tag{133}$$

and $W^* \equiv |g_c - g^*|$. In the example in Fig. 16, the crossover occurs at

$$W^* = 0.6 \times 10^{-7} t. \tag{134}$$

On the other hand, the free-energy expansion in Eq. (117) indicates that the crossover is given by

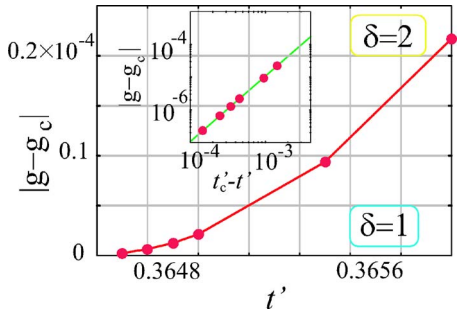

FIG. 15. (Color online) Crossover boundary between the $\delta=2$ region and $\delta=1$ region in the plane of $g-g_c$ and t'. The inset shows a log-log plot of the crossover in the plane of $|g-g_c|$ and t'_c-t'. The solid (green) line shows the result of a least-squares fitting near the MQCP by assuming the function $y=kx^2$, where $y=|g-g_c|$ and $x=|t'_c-t'|$.

$$W^*_{FE} \sim \frac{T^2}{a^2} t \sim \left(\frac{0.001}{13.48}\right)^2 t \sim 10^{-8} t, \tag{135}$$

where a is estimated in Eq. (126). They are consistent with each other.

For several choices of temperatures, the same analyses were performed and we determined the Ising region. We show the result in Fig. 17(a). In the free-energy expansion, the crossover W^* is expected asymptotically as $W^* \sim T^2$ at low temperatures. The scaling of W^* as a function of T appears to show a somewhat smaller exponent p than 2 for the fitting $W^* \sim T^p$. The origin of this discrepancy is likely to come from the temperature dependence in a. Except for this discrepancy, the order of the Ising region estimated from the Hartree-Fock calculations is consistent with that of the free-energy expansion.

Route (*b*). In the insulating region, we show the numerically obtained phase diagram for the crossover in Fig. 17(b). To obtain the crossover point from $\delta=3$ for the Ising region to $\delta=1$ for the MQCP, we have used a criterion different from the metallic side in route (a). The slope of Y as a function of W is not a monotonic function of W, and it crosses over first from $\delta=3$ to an even smaller value, after which it increases to $\delta=1$. To specify the crossover point, we have taken it as the point which shows the minimum slope in the crossover region. For example, at $T=0.001t$, W^* is estimated as

$$W^* = 2.23 \times 10^{-4} t. \tag{136}$$

The free-energy expansion indicates from Eq. (121) that the crossover point W^* for δ is given by

$$W^*_{FE} \sim \frac{T}{b} \sim \frac{0.001t}{0.99} \sim 10^{-3} t, \tag{137}$$

where b is estimated in Eq. (129). As far as the order of W, it indicates that the Hartree-Fock numerical results are consistent with that of the free-energy expansion. Figure 17(b) is obtained by performing the same analyses for several choices

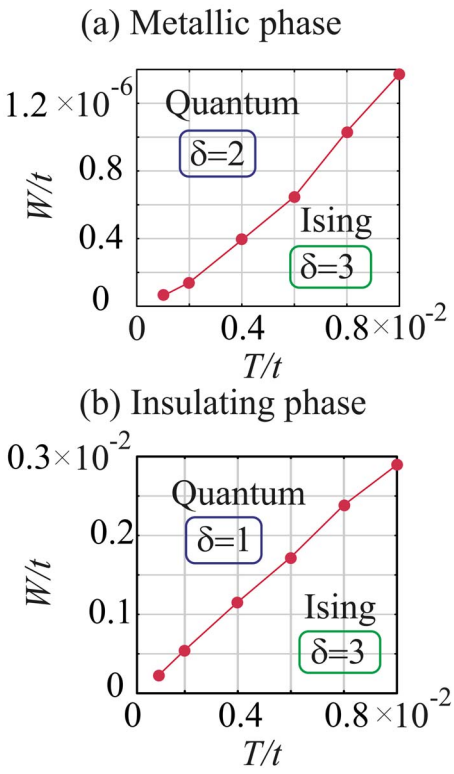

FIG. 17. (Color online) (a) Phase diagram of the crossover boundary between Ising and the quantum regions for δ in the metallic phase plotted in the plane of W/t and T/t. (b) Phase diagram of the crossover boundary between Ising and quantum regions for δ in the insulating phase plotted in the plane of W/t and T/t.

of temperature. The temperature dependence of the crossover is estimated as $W^* \sim T^{1.1}$. This is rather consistent with $W^* \sim T$ obtained from the free-energy expansion. It is likely that the slight discrepancy between the two results comes from the temperature dependence of b.

Route (c). We also discuss the crossover of the critical exponent β in route (c). For example, near the critical point at $T=0.001t$, β crosses over from 1 (MQCP) to 1/2 (Ising mean-field value) in a monotonic fashion. The crossover W^* is estimated by the same method as route (a) as

$$W^* = 0.000\,37 \sim 10^{-4}t. \tag{138}$$

In the free-energy expansion, the crossover is estimated from Eq. (123) as

$$W^*_{FE} \sim \frac{T}{c} = \frac{0.001t}{32.4} \sim 10^{-4}t, \tag{139}$$

where c is estimated in Eq. (132). The numerical Hartree-fock result is consistent with W^*_{FE}.

Figure 18 shows W at the crossover for several choices of temperatures. The temperature dependence of the Ising region is estimated as $W^* \sim T^{0.7}$, which has a somewhat smaller slope than $W^* \sim T$ expected from the free-energy expansion. Again, it is likely that the discrepancy comes from the temperature dependence of c. Numerical results suggest that we need to consider the overall temperature dependences of a, b, and c on the quantitative level. However, we do not go further into detail on this point. At least the existence of two critical regions governed by the MQCP and Ising classes is now well established with crossovers, which are qualitatively consistent with the free-energy expansion. The numerical results show how the asymptotic scaling for the location of the crossover derived in the free-energy expansion is modified in regions distant from the critical point.

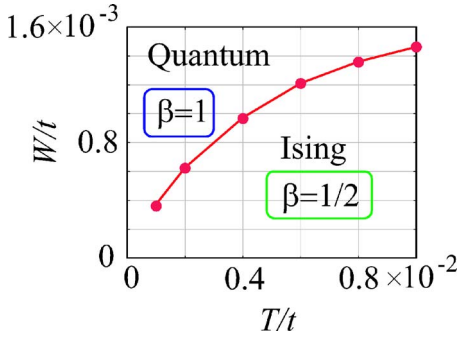

FIG. 18. (Color online) Crossover boundary for the critical exponent β plotted in the plane of W/t and T/t.

VI. COMPARISON WITH EXPERIMENTAL RESULTS

In real materials, strictly speaking, a well-defined Mott critical point has been observed so far only at finite temperatures, as we discuss below. There, Ising critical exponents should be observed in the region sufficiently close to the finite-temperature critical point. However, because the Ising region is not wide enough at low temperatures and crosses over to MQCP criticality, quantum critical exponents may be observed in actual experiments. Although we have to be careful in comparing our results for the very simple model with possible artifacts of the Hartree-Fock approximation with experimental results on more complicated systems, it may offer insight into the relevance of the quantum criticality. Here, we compare our results with the experimental results of κ-$(ET)_2Cu[N(CN)_2]Cl$ reported by Kagawa, Miyagawa, and Kanoda.[46] The critical exponents in the metallic phase show clear evidence of the crossover in our numerical results for δ and β. At $T_c=0.01t$ [see Fig. 17(a)], the classical Ising region is observed for $W<10^{-6}t$. This critical temperature is comparable to the experimental value $T_c \sim 40$ K with the estimated transfer $\sim 0.1-0.2$ eV obtained from a Hueckel calculation.[52] In κ-$(ET)_2Cu[N(CN)_2]Cl$, 1.0 MPa roughly corresponds to 0.001 t,[52,53] which is estimated from the pressure dependence together with the dependence on the anion species in the experimentally obtained phase diagram. The smallest distance from the critical point accessible in the experimental resolution is estimated as $|P-P_c| \sim 0.1$ MPa $\sim 10^{-4}$ t, which is much larger than 10^{-6} t suggested from the theoretical estimate above. This indicates that, in the experiments, the distance between the true critical point and the available point closest to it is two orders of magnitude larger than the distance of the crossover boundary from the critical point. This is consistent with the experimental result that the singularity of the conductivity is well fit only by the quantum

critical exponent $\delta=2$. Other exponents in this κ-ET compound show $\gamma=1$ and $\beta=1$. These are completely consistent with the present MQCP universality.

We have also obtained that δ in the insulating phase shows a crossover. The critical exponent δ changes into $\delta=3$ (Ising) from $\delta=1$ (MQCP). We estimate the Ising region as $W<W^*\sim 10^{-3}t$ for $T_c=0.01t$. This W^* corresponds to about 1.0 MPa by assuming that 1.0 MPa corresponds to $0.001t$. The Ising region in the insulating phase is much wider than that of the metallic phase. From this, we have more of a chance for observing the Ising region ($\delta=3$) in the experiments. The experimental result shows that effective charge gap Δ closes with the singularity as $\Delta\sim(P_c-P)^{0.4\pm0.1}$ in the insulating phase. This indicates that $\delta=2-3$. This critical exponent may be consistent with the Ising mean-field value $\delta=3$. If one were able to approach the Ising critical region ($|P-P_c|\ll 1.0$ MPa) in an organic conductor of the κ-ET compound, since the system is quasi-two-dimensional, the 2D Ising critical exponent $\delta=15$ should be obtained. It could show a crossover from the quantum exponent $\delta=1$ governed by the MQCP to the Ising mean-field value $\delta=3$ in the region closer to the critical point with an extremely narrow critical region of $\delta=15$. However, since the experimental data are obtained in the parameter space not close enough to the Ising region of the critical point, the mean-field critical exponent may be obtained similarly to the case of $(V_{1-x}Cr_x)_2O_3$.[44] Although the pressure dependence of the parameter value for the transfer is so far not available, a high critical temperature $\sim$450 K of $(V_{1-x}Cr_x)_2O_3$ likely enables the observation of the Ising criticality.

As we mentioned in Sec. I, some of the high-T_c cuprates such as $Bi_2Sr_2CaCu_2O_{8+y}$ and $(La,Sr)_2CuO_4$ show consistency with $\delta=2$, whereas some of other compounds such as $(Ca,Na)_2CuO_2Cl_2$ show a quicker shift, rather consistently with $\delta=1$. This variety suggests that parameter values of various copper oxides correspond to a diverse range from the region close to the MQCP to that deeply in the quantum critical line. The normal-state properties as well as the superconducting transition temperatures may depend on the distance from the MQCP, which is an intriguing issue left for the future. In the case of filling-control transitions, the first-order transition appears as an intrinsic instability to the phase separation. The phase separation is transformed to the electronic inhomogeneity with finite-size domains under the constraint of the long-range Coulomb interaction and the charge neutrality. The distance from the MQCP directly measures the tendency for instability toward such inhomogeneities. The diversity of the cuprate superconductors in terms of this tendency can be classified by this distance.

^{3}He adsorbed on a graphite surface offers a unique purely two-dimensional fermion system. In addition to the anomalous suppression of T_F that is consistent with $z=4$,[36] as mentioned in Sec. I, a recent detailed study at lower temperatures has revealed a richer structure in the specific heat.[54] The second layer of He approaches the registered phase (namely, a solid phase with commensurate periodicity to the first-layer solid at the density 4/7 in terms of the first layer density) with increasing He pressure. Near but below the density at the registered phase, the lower-temperature structure of the specific heat suggests that the large residual entropy expected from the large dynamical exponent $z=4$ is released below 10 mK. A strong crossover around 10% doping between low- and high-density regions is suggested from the transfer of the entropy release, where the release from the specific-heat peak structure at 10–100 mK for the lower-density (more than 10% doping) region is replaced with the release at lower temperatures around or less than 1 mK for the higher-density (less than 10% doping) region. The release at this low-temperature region may arise from the superposition of the contribution from carrier motion and spin, which originate from two different regions of the Brillouin zone, respectively, as analyzed by the electron differentiation in momentum space with a simplified two-fluid picture.[39] This transfer of the entropy-releasing temperature implies a drastic topological change of the Fermi surface in the ground state such as a Lifshitz transition to the small Fermi pocket or approximate arc structure. If a clear Lifshitz transition occurs, we expect a singular dependence of the thermodynamic properties on the density measured at low temperatures below 1 mK. Another conceivable case is that such a singular dependence is not observable when the topological change occurs in the pseudogap region with faint spectral weight out of the "arc." This may be analyzed by measuring the data at temperatures lower than 1 mK in more detail around this crossover, which is an intriguing issue left for future studies. If a Lifshitz transition occurs, the transition to the registered phase occurs also as a topological transition with vanishing Fermi pockets to the registered phase. So far, it is not clear whether the transition to the registered phase is eventually realized across the quantum critical line or near the MQCP, because lower-temperature data below 0.1 mK are not available.

The physics of electron differentiation tightly associated with the present unusual universality of metal-insulator (or liquid-registered phase) transitions is a common central issue of high-T_c cuprates and monolayer ^{3}He. The overall experimental indications show the relevance of the unusual quantum criticality around the MQCP. A more detailed analysis is left for future studies. Studies of the crossover effect beyond the Hartree-Fock approximation are also left for future studies.

VII. SUMMARY AND DISCUSSION

Quantum MI transitions between symmetry-broken metals and insulators have been studied within the Hartree-Fock approximation using the extended Hubbard model. By increasing the on-site Coulomb interaction U and nearest-neighbor Coulomb interaction V, this model at half filling has a tendency to charge ordering or antiferromagnetic ordering within the mean-field level. Preexisting gaps generated by such spontaneous symmetry breakings allow us to capture the essence of electron correlation effects on metal-insulator transitions. In this paper, we have mainly considered the case of charge ordering in the region $4V>U$. However, it is essentially the same for antiferromagnetic ordering in the region $U>4V$ and the present study can be easily extended, where the criticality does not change.

Using the Hartree-Fock free energy, we have studied the criticality of MI transitions. To clarify the nature of MI transitions, we have performed the free-energy expansion as

$$F_\Delta = F(\Delta_c) + AY + \frac{B}{2!}Y^2 + \frac{C}{3!}Y^3, \tag{140}$$

in terms of the gap amplitude measured from the MI transition point, $Y=\Delta_c-\Delta$. This free-energy expansion has an unconventional feature, where the coefficients B and C have different values between B_m and C_m in metals and B_i and C_i in insulators with jumps at the transition point $Y=0$. Although the expansion is not regular at $Y=0$, the Y dependence of F is regular in a piecewise analytic way in each metallic ($Y>0$) and insulating ($Y<0$) region separately, which makes the expansion unique. Because of the jump from $C_m>0$ to $C_i<0$ at $Y=0$, the whole expansion (140) up to cubic order of Y is bounded from below and the free-energy minimum appears at a finite Y. Such jumps of the coefficients at $Y=0$ clearly violate the Ginzburg-Landau-Wilson scheme of phase transitions and indicate that the MI transition at $T=0$ is not explained by the concept of spontaneous symmetry breaking. The origin of the jumps is ascribed to the jump of the density of states from a nonzero value in metals to zero in insulators in two dimensions. It reflects the topological nature of the MI transition, which is caused by the disappearance (or emergence) of the Fermi surface without a change in symmetry.

From the free-energy expansion in Eq. (140), we find that both continuous and first-order MI transitions occur at $T=0$. The numerical estimates for the relevant parameter region of the extended Hubbard model show $B_i>0$ and $B_i>B_m$, whereas $C_i<0<C_m$. When $B_m>0$, the region $A<0$ represents the metallic phase, while the insulating state is stabilized for $A>0$. For $B_m>0$, the MI transitions are always continuous. The quantum critical line with the continuous MI transition is determined by the condition $A=0$. When B_m becomes zero, the quantum critical line terminates at the marginal quantum critical point ($A=0$, $B_m=0$) and the first-order transition line begins in the region $B_m<0$. Our calculated coefficients A and B_m specify the locations of the MQCP at $t'=0.055\,71$ and $t'=0.364\,55$ for the extended Hubbard model.

In Sec. IV, we have studied the MI transitions by solving the self-consistent equation numerically. The obtained phase diagram in the $t'-g$ plane at $T=0$ contains two MQCP's. We have confirmed that the numerical results are consistent with the analytical results obtained in Sec. III.

Our mean-field exponents at the MQCP are essentially exact beyond the mean-field theory. Substituting these critical exponents into the Ginzburg criterion,[9] we obtain the upper critical dimensions d_c as

$$d_c = \frac{\gamma+2\beta}{\nu} - z = 2.$$

Since the two-dimensional system is at the upper critical dimension, the mean-field critical exponents of the MQCP should be exact except for possible logarithmic corrections.

Using the free-energy expansion in Eq. (140), we obtain the critical exponents of the MQCP as $\alpha=-1$, $\beta=1$, $\gamma=1$, $\delta=2$, $\nu=1/2$, and $\eta=0$ and the dynamical exponent $z=4$ in the metallic side of the transition. These critical exponents show that the MQCP belongs to an unconventional universality class different from those obtained from phase transitions caused by spontaneous symmetry breaking.

The discontinuities of the coefficients B and C exist, in the strict sense, only at $T=0$. At nonzero temperatures, the jump is immediately smeared out, which makes a crossover to a different universality. We find that the first-order MI transition boundary extends to nonzero temperatures and terminates at the critical point. Around the finite-temperature critical line, the free energy follows the GLW scheme. The criticality is perfectly categorized by the Ising universality. This means that the universality class of the finite-temperature transition may be characterized as a symmetry breaking transition in contrast to $T=0$ transitions.

The peculiarity of the universality at the MQCP is ascribed to the fact that the MQCP appears as the marginal point between the conventional GLW transition at nonzero temperature with emergence of the spontaneous symmetry breaking and the topological transition at $T=0$, each of which is described by already known physics, while its connecting point is not. This unconventional universality class of the MQCP is consistent with recent experimental results of κ-$(ET)_2Cu[N(CN)_2]Cl$. Although we have focused on the bandwidth-control MI transitions, these critical exponents are the same as those of the filling-control MI transitions.

We have clarified how the crossover between Ising and MQCP universalities appears. It has been shown that even the finite-temperature critical point may show the MQCP region when the parameter is tuned away from the narrow Ising region. This explains the experimental observation on the κ-ET compound.

In this paper, we have considered only MI transitions in the ordered phase. We assume that a preexisting gap exists in the metallic phase because of the symmetry breaking. However, beyond the mean-field theory, even without the symmetry breaking, a preexisting gap opens in the metallic phase as in the case of Mott insulators at low dimensions. Therefore, the consequence of the present mean-field treatment may survive without a strict order, where Δ may be replaced with the correlation-induced gap without long-range order. This is indeed corroborated by various numerical studies performed beyond the mean-field approximations, which consistently support the hyperscaling with $\delta=2$ and $z=4$.

The present results show that the MI transition is governed by the topological change of the Fermi surface, with shrinkage (or emergence) at selected momentum points. This is different from other types of mean-field theories such as the dynamical mean-field approximations, where the MI transition is governed instead by the vanishing renormalization factor Z. On the verge of the MI transition in the metallic side, it possibly means that the Fermi surface is reduced to small pockets, which violates the Luttinger sum rule. If the system undergoes a Lifshitz transition from a large to small Fermi surface in the metallic phase, this violation is allowed on the side of small pockets. The improvement of the dynamical mean-field theory to include the momentum

dependence indeed suggests the existence of such a Lifshitz transition as we discussed in Sec. I. The existence of the small Fermi surface without folding of the Brillouin zone in the absence of translational symmetry breaking is a fundamental issue and should be more thoroughly studied in the future.

The present study has revealed a mechanism of generating a quantum critical point of the metal-insulator transition, which has been unexplored in the literature. The MQCP emerges because of the generation of the gap determined in cooperation with the kinetic energy gain of metallic carriers. Its combined and nonlinear effect yields pinning of the quasiparticle energy in contrast to the rigid-band picture. This may be expressed by an attractive effective interaction of carriers. It generates an unconventional universality.

A remarkable finding is that the MQCP is governed by the coexistence of quantum fluctuations and the divergence of the density fluctuations at small wave numbers. Such density fluctuations may cause various further and deeper effects near the MQCP. Its thorough understanding is an intriguing issue left for future studies. Among all, revealing momentum- and frequency-resolved density fluctuations is an extremely important, challenging issue of experimental studies, which must reveal an anomalous and critical enhancement near the MQCP as well as near the finite-temperature critical point if accurate measurements are made. Thorough studies of the superconducting mechanism arising from the MQCP[40] are also an extremely important issue to be explored.

ACKNOWLEDGMENTS

The authors are indebted to Youhei Yamaji for extensive discussions. The authors thank Hiroshi Fukuyama, Kazushi Kanoda, and Fumitaka Kagawa for illuminating discussions on their experimental results. One of the authors (T.M.) thanks Shinji Watanabe for stimulating discussions. This work is supported by Grant-in-Aids for Scientific Research on Priority Areas under Grants Nos. 17071003 and 16076212 from MEXT, Japan. A part of our computation in this work has been done using the facilities of the Supercomputer Center, Institute for Solid State Physics, University of Tokyo.

APPENDIX A

In this appendix we show details of the numerical calculations. In the standard procedure of solving Eqs. (46) and (47), the input parameters are the effective interaction g and particle density n. In this procedure, the chemical potential μ and the order parameter m are determined by solving Eqs. (46) and (47) self-consistently. This procedure costs much computation time and is not efficient in determining μ and m precisely.

Instead, we use a different procedure. Namely, we take Δ and n as input parameters, while the output parameters are g and μ. By following this procedure, first, in Eq. (47) for fixed Δ, we can determine the chemical potential μ to satisfy the condition $n=1$ independent of Eq. (46). Then, using this μ, we perform the integration of the right-hand side of Eq. (46) and obtain g. Finally, we obtain the order parameter $m=\Delta/g$. Since this procedure does not require self-consistent calculations, it is possible to calculate Eqs. (46) and (47) rapidly and precisely.

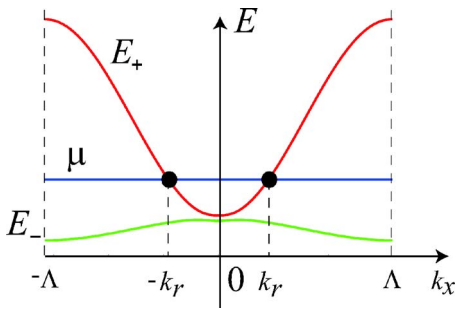

FIG. 19. (Color online) Schematic band structure for fixed k_y. Circles represent the crossing points of the upper band and the chemical potential, which occur at k_r.

Hereafter, we explain the details of the integration of Eqs. (46) and (47). To calculate the k-space integration in Eq. (47), first we fix k_y and obtain the particle density integrated over k_x: namely, $n(k_y)$. It is easy to solve the equation

$$\xi_2(k_x,k_y) \pm \sqrt{\xi_1(k_x,k_y)^2 + \Delta^2} - \mu = 0, \tag{A1}$$

with respect to $\cos k_x$ for fixed k_y analytically since the equation is quadratic with respect to $\cos k_x$. Using the roots of the Eq. (A1), we obtain $n(k_y)$ exactly. To simplify the explanation, we only consider the case that the two real roots exist for upper band and their absolute values are less than 1. In this case, analytically we can obtain the location of the point where E_+ and μ cross: namely, k_r and $-k_r$ (see Fig. 19). From this, for the upper [lower] band, the particle density for fixed k_y is given by $n(k_y)_+=2k_r/2\pi$ $[n(k_y)_-=2\Lambda(k_y)/2\pi]$, where $\Lambda(k_y)$ is the edge of the Brillouin zone. The particle density for fixed k_y is given as $n(k_y)=n(k_y)_+ + n(k_y)_-$. In other cases, in a similar way, we can obtain $n(k_y)$ analytically. By integrating $n(k_y)$ over k_y, we obtain the whole particle density n. Along the k_y direction, we use the Newton-Cotes formula and take the number of points in the k_y direction up to 400 000.

Next, we explain the way of integrating over k on the right-hand side of Eq. (46). We fix k_y and perform the k_x integration first. Along the k_x direction, we use double-exponential (DE) formula, which is suitable for the integration of the analytic function in the integration period. It is known that the DE formula is one of the optimized methods to integrate the analytic function with the highest accuracy using the smallest number of points. In the above case, integration periods I_1 and I_2 are given as $I_1=[-\Lambda,-k_r]$ and $I_2=[k_r,\Lambda]$ (see Fig. 19). The DE formula is useful in these periods, since the right-hand side of Eq. (46) is analytical. We take the number of points in these periods up to 1000. Then we perform the integration over k_y using the Newton-Cotes formula and obtain the effective interaction g. We take the number of points in the k_y direction up to 400 000 for the integration.

APPENDIX B

In this appendix we derive Eqs. (63)–(65). First, we obtain the density of states (DOS) at the bottom (top) of the upper (lower) band, respectively.

The location of the bottom of the upper band is given by $(\pi,0)$ and $(0,\pi)$. Near $(\pi,0)$, using Eq. (44), E_+ is expanded with respect to $q_x=k_x-\pi$ and $q_y=k_y$ as

$$E_+ \sim -4t' \cos q_x \cos q_y + \sqrt{4t^2(\cos q_x - \cos q_y)^2 + \Delta^2} - \mu \tag{B1}$$

$$\sim -4t' + \Delta + 2t'q^2 - \mu, \tag{B2}$$

where we define $q=\sqrt{q_x^2+q_y^2}$. From this, we obtain

$$\frac{dE_+}{dq} \sim 4qt'. \tag{B3}$$

The DOS of the upper band near $(\pi,0)$ is given by

$$D_+ = \frac{1}{4\pi t'}. \tag{B4}$$

Near the MI transition, the Fermi wave number q_+ is determined by the condition

$$E_+ \sim -4t' + \Delta + 2t'q_+^2 - \mu = 0, \tag{B5}$$

where μ is the chemical potential. From Eqs. (B2) and (B5), we obtain

$$q_+ \sim \sqrt{\frac{2\Delta_c - \Delta + \mu}{\Delta_c}}, \tag{B6}$$

where $\Delta_c=2t$. Using this, the electron density of the upper band—namely, the electron density X_+—including the spin degeneracy is given by

$$X_+ = \frac{q_+^2}{2\pi} = \frac{1}{2\pi}\left(\frac{2\Delta_c - \Delta + \mu}{\Delta_c}\right). \tag{B7}$$

The location of the top of the lower band is given by $(\pi/2,\pi/2)$ and its equivalent points. Near $(\pi/2,\pi/2)$, using Eq. (44), E_- is expanded with respect to $q_x=\pi/2-k_x$ and $q_y=\pi/2-k_y$, which leads to

$$E_- \sim -\Delta + 2q^2\left(t' \sin 2\theta - \frac{t^2(1+\sin 2\theta)}{\Delta_c}\right) - \mu, \tag{B8}$$

where we define $q=\sqrt{q_x^2+q_y^2}$. Then we obtain

$$\frac{dE_-}{dq} \sim -4q\left[\frac{t^2}{\Delta_c} - \left(t' - \frac{t^2}{\Delta_c}\right)\sin 2\theta\right]. \tag{B9}$$

From Eq. (B9), the DOS of the lower band near $(\pi/2,\pi/2)$ is given by

$$D_- = \frac{8}{(2\pi)^2}\int_{3\pi/4}^{7\pi/4} \frac{d\theta}{4[t^2/\Delta_c - (t' - t^2/\Delta_c)\sin 2\theta]} = \frac{1}{2\pi\sqrt{t^2 - t'^2}}. \tag{B10}$$

Near the MI transition, the Fermi wave number q_- is determined by the condition

$$E_- \sim -\Delta + 2q_-^2\left(t' \sin 2\theta - \frac{t^2(1+\sin 2\theta)}{\Delta_c}\right) - \mu = 0, \tag{B11}$$

where μ is the chemical potential. From Eqs. (B8) and (B11), we obtain

$$q_-(\theta) \sim \sqrt{\frac{t'(-\mu-\Delta)}{t^2 - (2t'^2 - t^2)\sin 2\theta}}. \tag{B12}$$

Using this, the hole density of the lower band—namely, the hole density X_-—is given by

$$X_- = \frac{4}{4\pi^2}\int_{3\pi/4}^{7\pi/4} q_-^2 d\theta = \frac{(-\mu-\Delta)}{2\pi\sqrt{t^2 - t'^2}}. \tag{B13}$$

At half filling, X_+ should be equal to X_-. From this condition, recalling Eq. (63) and using Eqs. (B7) and (B13), we obtain $\tilde{\alpha}$ as

$$\tilde{\alpha} = \frac{2t' - \sqrt{t^2 - t'^2}}{2t' + \sqrt{t^2 - t'^2}}. \tag{B14}$$

*Electronic address: misawa@solis.t.u-tokyo.ac.jp

[1] M. Imada, A. Fujimori, and Y. Tokura, Rev. Mod. Phys. **70**, 1039 (1998).
[2] M. Imada, J. Phys. Soc. Jpn. **63**, 4294 (1994).
[3] M. Imada, J. Phys. Soc. Jpn. **64**, 2954 (1995).
[4] L. S. Ornstein and F. Zernike, Proc. K. Ned. Akad. Wet. **17**, 793 (1914).
[5] A. Einstein, Ann. Phys. (Leipzig) **33**, 1275 (1910).
[6] M. Smoluchowski, Ann. Phys. (Leipzig) **25**, 205 (1908).
[7] L. D. Landau, E. M. Lifshitz, and E. M. Pitaevskii, *Statistical Physics* (Butterworth Heinemmann, New York, 1999).
[8] K. G. Wilson, Rev. Mod. Phys. **55**, 583 (1983).
[9] For a textbook, see N. G. Goldenfeld, *Lectures on Phase Transitions and Renormalization Group* (Addison-Wesley, Reading, MA, 1992).
[10] R. J. Elliott, J. Phys. C **4**, 2359 (1971).
[11] T. Moriya, *Spin Fluctuations in Itinerant Electron Magnetism* (Springer-Verlag, Berlin, 1985).
[12] J. A. Hertz, Phys. Rev. B **14**, 1165 (1976).
[13] A. J. Millis, Phys. Rev. B **48**, 7183 (1993).
[14] A. J. Millis, A. J. Schofield, G. G. Lonzarich, and S. A. Grigera, Phys. Rev. Lett. **88**, 217204 (2002).
[15] X.-G. Wen, Ann. Phys. (N.Y.) **316**, 1 (2005).
[16] J. Hubbard, Proc. R. Soc. London, Ser. A **276**, 238 (1963); **227**, 237 (1964); **281**, 401 (1964).
[17] W. F. Brinkman and T. M. Rice, Phys. Rev. B **2**, 4302 (1970).
[18] A. Georges, G. Kotliar, W. Krauth, and M. J. Rozenberg, Rev. Mod. Phys. **68**, 13 (1996).

[19] S. Onoda and M. Imada, Phys. Rev. B **67**, 161102(R) (2003).
[20] K. Hanasaki and M. Imada, J. Phys. Soc. Jpn. **75**, 084702 (2006).
[21] S. Onoda and M. Imada, J. Phys. Chem. Solids **63**, 2225 (2001).
[22] M. Imada and S. Onoda, J. Phys. Chem. Solids **62**, 47 (2002).
[23] T. Yoshida, X. J. Zhou, T. Sasagawa, W. L. Yang, P. V. Bogdanov, A. Lanzara, Z. Hussain, T. Mizokawa, A. Fujimori, H. Eisaki, Z.-X. Shen, T. Kakeshita, and S. Uchida, Phys. Rev. Lett. **91**, 027001 (2003).
[24] N. P. Armitage, F. Ronning, D. H. Lu, C. Kim, A. Damascelli, K. M. Shen, D. L. Feng, H. Eisaki, Z.-X. Shen, P. K. Mang, N. Kaneko, M. Greven, Y. Onose, Y. Taguchi, and Y. Tokura, Phys. Rev. Lett. **88**, 257001 (2002).
[25] C. Berthod, T. Giamarchi, S. Biermann, and A. Georges, Phys. Rev. Lett. **97**, 136401 (2006).
[26] M. Civelli, M. Capone, S. S. Kancharla, O. Parcollet, and G. Kotliar, Phys. Rev. Lett. **95**, 106402 (2005).
[27] Th. A. Maier, Th. Pruschke, and M. Jarrell, Phys. Rev. B **66**, 075102 (2002).
[28] For instance, in Refs. 1 and 3, the control parameter was taken as $\mu-\mu_c$, while here it is taken as g, which turns out to be scaled by $(\mu-\mu_c)^{1/2}$ for the MQCP of the filling-control transition in two dimensions. This makes a trivial factor of 2 necessary for the present $\nu=1/2$ in comparison with $\nu=1/4$ in Refs. 1 and 3, although z is commonly 4. Along the quantum critical line, this factor of 2 is not necessary, because $\mu-\mu_c$ is scaled linearly with g. The scaling between g and ζ will be clarified in Sec. II. The exponent $\alpha=2-(d+z)\nu$ in the present definition is $\alpha=2-(d+z)/2$ while it is $\alpha=2-(d+z)/4$ in Refs. 1 and 3. In any case, these transformations do not make any difference in the scalings of real physical quantities.
[29] N. Furukawa and M. Imada, J. Phys. Soc. Jpn. **60**, 3604 (1991).
[30] N. Furukawa and M. Imada, J. Phys. Soc. Jpn. **61**, 3331 (1992).
[31] N. Furukawa and M. Imada, J. Phys. Soc. Jpn. **62**, 2557 (1993).
[32] M. Kohno, J. Phys. Soc. Jpn. **55**, 1435 (1997).
[33] S. Watanabe and M. Imada, J. Phys. Soc. Jpn. **73**, 1251 (2004).
[34] N. Harima, A. Fujimori, T. Sugaya, and I. Terasaki, Phys. Rev. B **67**, 172501 (2003).
[35] H. Yagi, T. Yoshida, A. Fujimori, Y. Kohsaka, M. Misawa, T. Sasagawa, H. Takagi, M. Azuma, and M. Takano, Phys. Rev. B **73**, 172503 (2006).
[36] A. Casey, H. Patel, J. Nyéki, B. P. Cowan, and J. Saunders, Phys. Rev. Lett. **90**, 115301 (2003).
[37] H. Nakano and M. Imada, J. Phys. Soc. Jpn. **68**, 1458 (1999).
[38] H. Tsunetsugu and M. Imada, J. Phys. Soc. Jpn. **67**, 1864 (1998).
[39] M. Imada, J. Phys. Soc. Jpn. **73**, 1851 (2004).
[40] M. Imada, J. Phys. Soc. Jpn. **74**, 859 (2005).
[41] M. Imada, Phys. Rev. B **72**, 075113 (2005).
[42] G. Kotliar, E. Lange, and M. J. Rozenberg, Phys. Rev. Lett. **84**, 5180 (2000).
[43] C. Castellani, C. Di Castro, D. Feinberg, and J. Ranninger, Phys. Rev. Lett. **43**, 1957 (1979).
[44] P. Limelette, A. Georges, D. Jerome, P. Wzietek, P. Metcalf, and J. M. Honig, Science **302**, 89 (2003).
[45] F. Kagawa, T. Itou, K. Miyagawa, and K. Kanoda, Phys. Rev. B **69**, 064511 (2004).
[46] F. Kagawa, K. Miyagawa, and K. Kanoda, Nature (London) **436**, 534 (2005).
[47] T. Misawa, Y. Yamaji, and M. Imada, J. Phys. Soc. Jpn. **75**, 083705 (2006).
[48] H. Kondo and T. Moriya, J. Phys. Soc. Jpn. **65**, 2559 (1996).
[49] W. Hofstetter and W. Vollhardt, Ann. Phys. (Leipzig) **7**, 48 (1998).
[50] The critical exponent β also characterizes the singularity of the order parameter with respect to the control parameter. Namely, we can define β as $X \propto a^{\beta}$, where X is the order parameter and a is a control parameter. In this definition, β is well defined even in the case of continuous MI transitions. In this case, since the control parameter is equivalent to the external field, β is equal to δ ($\beta=\delta=1$). In Ref. 41, this definition is chosen.
[51] A detailed derivation will be given elsewhere.
[52] T. Mori, H. Mori, and S. Tanaka, Bull. Chem. Soc. Jpn. **72**, 179 (1999).
[53] K. Miyagawa, K. Kanoda, and A. Kawamoto, Chem. Rev. (Washington, D.C.) **104**, 5635 (2004).
[54] Y. Matsumoto, D. Tsuji, S. Murakawa, H. Akisato, H. Kambara, and H. Fukuyama, J. Low Temp. Phys. **138**, 271 (2005).